E&G Quaternary Sci. J., 75, 85–105, 2026
https://doi.org/10.5194/egqsj-75-85-2026

Open Access E&G Quaternary Science Journal

Research article

An MIS 8 terrestrial record retrieved from a glacially overdeepened basin in the northern foreland of the European Alps

Gustav Firla[1], Christopher Lüthgens[1], Thomas Burschil[2], Stephanie Neuhuber[1], Roberta Pini[3], Oscar Marchhart[4], Alexander Wieser[4], Clemens Schmalfuss[1], Ernst Kroemer[5], and Markus Fiebig[1]

[1]Institute of Applied Geology, University of Natural Resources and Life Sciences Vienna (BOKU), Vienna, 1190, Austria
[2]Federal Institute for Geosciences and Resources (BGR), Hanover, 30655, Germany
[3]CNR IGAG, Laboratory of Palynology and Palaeoecology, Milano, 20126, Italy
[4]Isotope Physics, University of Vienna, Vienna, 1090, Austria
[5]Bavarian Environment Agency (LfU), Hof/Saale, 95030, Germany

Correspondence: Gustav Firla (gustav.firla@boku.ac.at)

Relevant dates: Received: 20 March 2025 – Revised: 13 October 2025 – Accepted: 29 January 2026 – Published: 19 March 2026

How to cite: Firla, G., Lüthgens, C., Burschil, T., Neuhuber, S., Pini, R., Marchhart, O., Wieser, A., Schmalfuss, C., Kroemer, E., and Fiebig, M.: An MIS 8 terrestrial record retrieved from a glacially overdeepened basin in the northern foreland of the European Alps, E&G Quaternary Sci. J., 75, 85–105, https://doi.org/10.5194/egqsj-75-85-2026, 2026.

Abstract: Sediments preserved in glacially overdeepened structures can provide a record of the regional Pleistocene glacial dynamics beyond the last glaciation. In order to unravel the glacial dynamics of the Isar-Loisach paleo-glacier, a cored sedimentary succession (ICDP-DOVE 5068_3_A) from an overdeepened basin near Schäftlarn, south of Munich, Germany, and an outcrop in its northern foreland ("Münchner Klettergarten" near Baierbrunn, on the southern margin of the Munich gravel plain, the "Münchner Schotterebene") were investigated with a multi-method approach. This approach focused on single-grain feldspar luminescence dating to establish a chronological framework and on a comprehensive geophysical survey to better understand the morphology of the overdeepened basin. The Schäftlarn core is generally divided into a fine-grained basal section and a coarse-grained top section. The filling of the fine-grained basal section started in early Marine Isotope Stage (MIS) 8. The basal part of the overlying coarse-grained sediment can be attributed to late MIS 8. The "Münchner Klettergarten" outcrop to the north exhibited a similar depositional age dating to late MIS 8 and therefore corresponding to the basal part of the coarse-grained sediment in Schäftlarn. The geophysical survey revealed two cross-cutting glacial basins, with the MIS 8 basin being cut by a younger basin of undetermined age. Based on the luminescence dating results and the geophysical survey, a mid-Pleistocene landscape development model of the Isar-Loisach paleo-glacier region is presented.

Kurzfassung: Sedimente, die in glazial übertieften Strukturen erhalten geblieben sind, können Informationen über die regionale Gletscherdynamik des Pleistozäns vor dem letzten Glazialzyklus geben. Um die Gletscherdynamik des Isar-Loisach Paläogletschers zu entschlüsseln, wurden eine gekernte sedimentäre Abfolge (ICDP-DOVE 5068_3_A) aus einem übertieften Becken bei Schäftlarn südlich

von München, Deutschland, und ein Aufschluss in seinem nördlichen Vorland ("Münchner Klettergarten" bei Baierbrunn, am südlichen Rand der Münchner Schotterebene) mit einem multimethodischen Ansatz untersucht. Dieser Ansatz fokussiert sich auf die Einzelkorn Feldspat Lumineszenzdatierung zur Erstellung eines chronologischen Rahmens und auf eine umfassende geophysikalische Untersuchung, um die Morphologie des übertieften Beckens darzustellen und dessen Genese besser zu verstehen. Der Schäftlarn-Kern ist grob in einen feinkörnigen unteren Abschnitt und einen grobkörnigen oberen Abschnitt unterteilt. Die Füllung des feinkörnigen unteren Abschnitts begann im frühen Marinen Isotopenstadium (MIS) 8. Der unterste Teil des darüber liegenden grobkörnigen Sediments kann dem späten MIS 8 zugeordnet werden. Der nördlich gelegene Aufschluss "Münchner Klettergarten" wies eine ähnliche Sedimentologie und ein Ablagerungsalter auf, das auf das späte MIS 8 datiert wurde und somit dem untersten Teil des grobkörnigen Sediments in Schäftlarn entspricht. Geophysikalische Untersuchungen entdeckten zwei sich schneidende Übertiefungen. Das MIS-8 Übertiefungsbecken wird von einem jüngeren Becken unbestimmten Alters durchschnitten. Auf Grundlage der Lumineszenzdatierungsergebnisse und der geophysikalischen Untersuchung wird ein mittelpleistozänes Landschaftsentwicklungsmodell für die Region des Isar-Loisach Paläogletscher präsentiert.

1 Introduction

Overdeepened basins are erosional structures found below the present landscape surface in areas affected by former glaciations. In overdeepenings, the erosion reaches below the fluvial base level of the drainage system. It has been assumed that the acting erosional forces are predominantly driven by a combination of glacial erosion and erosion by pressurised sediment-laden subglacial meltwater (Preusser et al., 2010). The infill of these sediment traps can be used as an archive of Pleistocene glaciation history and landscape development (Buechi et al., 2024), because overdeepened basins are thought to encompass nested sedimentary sequences from different glacial and interglacial phases. The DOVE (Drilling Overdeepened Alpine Valleys) research project set out to quantify the age, extent and environmental impact of Alpine glaciations (Anselmetti et al., 2022). This is going to be achieved by investigating complementing overdeepened structures along the northern part of the Alps. The analysis of a drill core in each selected overdeepening combined with geophysical surveys will provide data on the scale of a whole mountain range. The Quaternary subdivision of the Northern Alpine Foreland (Fig. 1a) is not uniform. Political entities that constitute this region use different systems to differentiate between glaciations. The Quaternary stratigraphical subdivision of Austria and Bavaria is morpho-stratigraphically organised with aspects of litho-facies added. This is mainly expressed using terrace levels and their assignment to different glaciations. The chronology of the glaciations varies between Austria (Reitner, 2022) and Bavaria (Doppler et al., 2011) (i.e. the association of glaciations to MIS is not coherent between Austria and Bavaria). The stratigraphy of Baden-Württemberg is organised around basin generations representing erosion cycles attributed to different glaciations (Ellwanger et al., 2011). Additionally, a terrace stratigraphy comparable to Austria and Bavaria is used. The Quaternary subdivision of northern Switzerland is based on a combination of different terrace levels, which represent different glaciations, as well as the infill of basins, which is also attributed to different glaciations (Preusser et al., 2011). One goal of ICDP-DOVE is to contribute to the unification of the Quaternary subdivision of the Northern Alpine Foreland across political borders. This study presents an investigation into an ICDP-DOVE site to the south of Munich, Germany, within the Isar-Loisach paleo-glacier region (Fig. 1b, c) and a glaciofluvial outcrop to the north near Baierbrunn ("Münchner Klettergarten") (Fig. 1d). The Baierbrunn outcrop and Schäftlarn are located on the southern margin of the Munich gravel plain ("Münchner Schotterebene"). In contrast to the terrace stratigraphic order, whereby the oldest terrace generation is situated at the highest elevation and the youngest terrace generation is located at the lowest elevation, the Munich gravel plain exhibits stratigraphic superposition (Doppler et al., 2011). Numerical chronological control for the Munich gravel plain is missing beyond MIS 6 (Klasen, 2008). This investigation, which encompasses multiple methods, will shed further light on the following research questions:

- When did deposition into the overdeepened structure start?
- How has the landscape in the investigated area developed?
- What information can be derived about the sedimentary dynamics between the overdeepened basin and its surroundings?

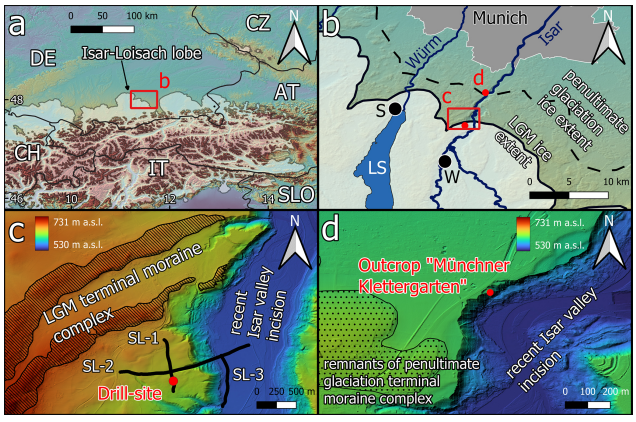

Figure 1. **(a)** General overview over the European Alps and their northern foreland. **(b)** Overview of the investigated area south of Munich (LS = Lake Starnberg, S = Starnberg, W = Wolfratshausen) with the maximum ice extent during the LGM (solid line) and the penultimate glaciation (dashed line) as defined by morphological features. **(c)** The area surrounding the drill site, with the terminal moraine complex indicated by the hatched area and the position of the three reflection seismic profiles (SL-1, SL-2, SL-3) as black lines. **(d)** The surrounding area of the investigated outcrop Baierbrunn ("Münchner Klettergarten"). The Copernicus European Digital Elevation Model (DEM) v1.0 (25 m resolution) was used as the base map for **(a)** and **(b)**. For **(c)** and **(d)**, the 1 m resolution DEM was provided by the Bayerische Vermessungsverwaltung.

2 Regional setting

The Northern Alpine Foreland (Fig. 1a, b) witnessed repeated Pleistocene glaciations, and it has been the focus of Quaternary research since the late 19th century. It was here that Penck and Brückner (1909) developed their glacial series model. In 2017, the Bavarian Environment Agency (LfU) retrieved a drill core (Bavarian Environment Atlas reference number: 8034BG015807; 5316031° N, 683597° E; 644 m a.s.l.) from an overdeepened basin near Schäftlarn, south of Munich (Germany), as a contribution to ICDP-DOVE (5068_3_A) (Fig. 1c). The drill core retrieved 198.8 m of Quaternary sediments (Fig. 2). The investigated overdeepening presented here is a branch basin of what was described by Jerz (1979) as the basin of Wolfratshausen. It is located in the ablation area of the former Isar-Loisach foreland glacier lobe (Fig. 1b). The bedrock is composed of Paleogene-Neogene Molasse sediments. To the south lies the folded Molasse formation (Faltenmolasse) followed by Alpine Nappes (Doben et al., 1996). The drill site is located ∼ 1 km south of the Last Glacial Maximum ice-marginal position defined by morphological features (i.e. terminal moraine) (Doppler et al., 2011). To the east of the drill site, the recent Isar Valley is incised into Pleistocene sediments with Molasse bedrock outcropping at the base of the valley slope in some places (Jerz et al., 1987). To the west, Lake Starnberg provides an example of an overdeepening that has not yet been entirely filled with sediments (Gegg and Preusser, 2023).

To better understand the local paleo-glacial dynamics and the depositional chronology in the glacier foreland, a prominent glaciofluvial outcrop ∼ 6.5 km north-east of the drill-site near Baierbrunn, colloquially called "Münchner Klettergarten" was investigated (5322298° N 686086° E; 580 m a.s.l. – LfU geotope no. 184002) (Fig. 1d and Fig. S1 in the Supplement). It was described by Penck and Brückner (1909) as a threefold division of glaciofluvial sediments into low terrace deposits (Niederterrassen Schotter), high terrace deposits (Hochterrassen Schotter) and Munich cover gravel deposits (Münchner Deckenschotter) overlying each other in superposition (Fig. 3). Jerz (1993) attributed the basal glaciofluvial deposits to either the Donau or Günz glaciation.

3 Methods

3.1 Core logging

The wet bulk density, magnetic susceptibility and natural gamma radiation were measured on the still-sealed whole round drill cores using a Geotek Multi-Sensor Core Logger (MSCL) at the drill core storage facility of the Federal Institute for Geosciences and Natural Resources (BGR) in Berlin-Spandau, Germany. Wet bulk density measurements were conducted for a section at the bottom and top of the core. Magnetic susceptibility and natural gamma radiation were measured over the whole depth of the core except for the diamictic section at the top. The drill cores were split into an archive half and a half used for sampling and photo documentation at the drill core storage facility of the Bavarian Environment Agency (LfU) in Hof, Germany. Visual sedimentological and structural logging was conducted. The fine-grained section of the drill core was sampled every meter for grain-size analysis, and organic and inorganic carbon measurements. Grain-size measurements were conducted on a Malvern Panalytical Mastersizer 3000 at the University of Freiburg. Total carbon and total inorganic carbon were measured at the University of Bern using a Thermo Scientific FLASH 2000 Elemental Analyzer. Total inorganic carbon was derived by subtracting the total organic carbon values from the total carbon values.

3.2 Luminescence dating

Luminescence dating was conducted on eight samples (VLL-0553-L to VLL-0560-L) from the 5068_3_A Schäftlarn drill core (Fig. 2) and on four samples (VLL-0643-L, VLL-0644-L, VLL-0645-L and VLL-0648-L) from the outcrop Baierbrunn (Fig. 3). Luminescence samples from core 5068_3_A can be grouped into two clusters. One cluster consist of five samples from the base of the core (unit A1: 198–189 m) to constrain the start of the infilling of the overdeepened struc-

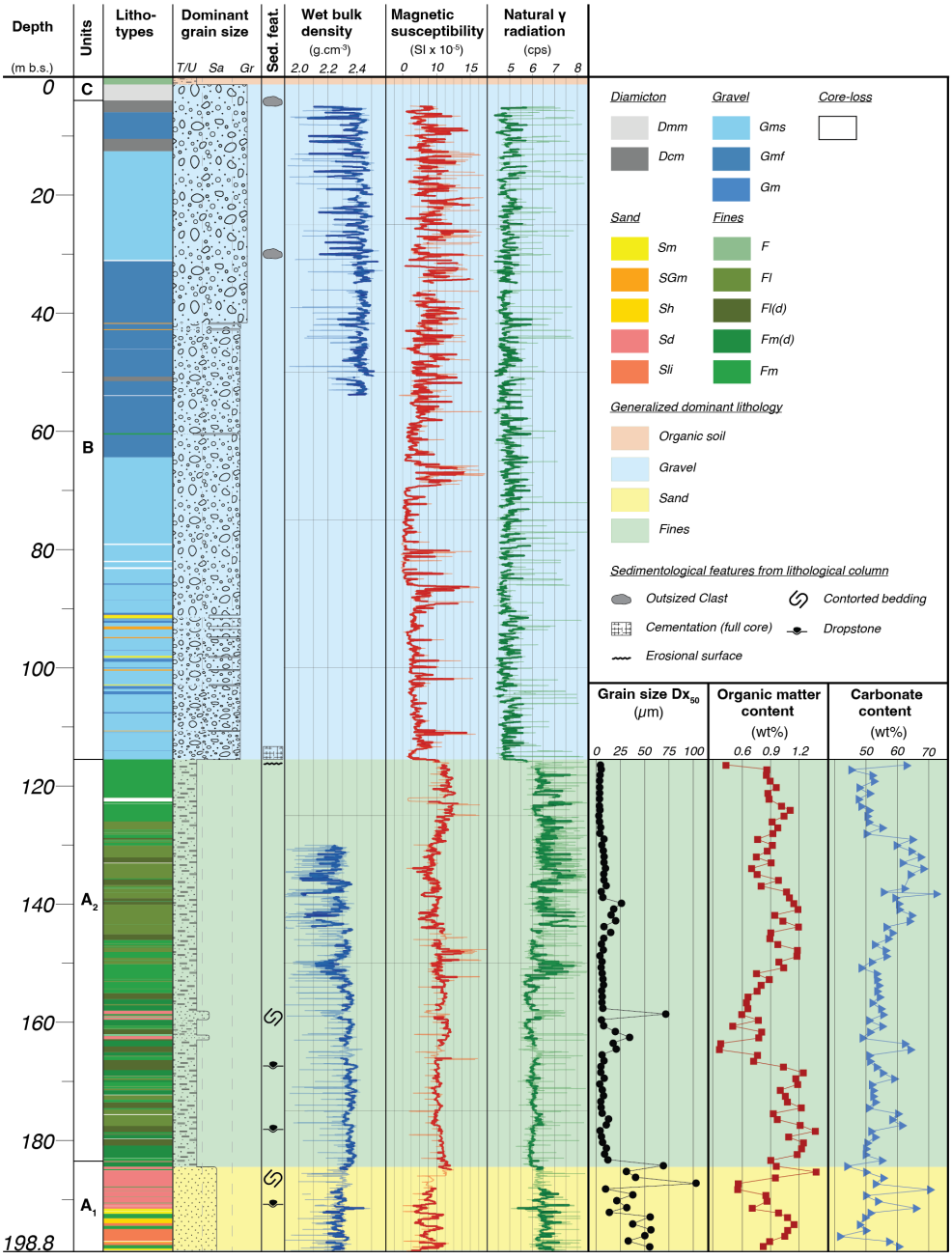

Figure 2. Core overview from left to right: stratigraphic column with lithofacies associations after Schaller et al. (2023) and Schuster et al. (2024), MSCL data (reliable data in bold), average grain-size, organic matter content and carbonate content.

ture. Samples of the second cluster were taken from sand layers in unit B (102–91 m). Two samples from the Baierbrunn outcrop were taken from the same strata ~ 20 m apart from each other. VLL-0643-L (Fig. 3b BB2) was sampled using a conventional steel tube but with considerable difficulties due to the cementation of the material. This resulted in mixing of bleached and unbleached material in the tube, which was already noted during sampling. Because of this, VLL-0644-L (Fig. 3b BB2) was sampled as a sediment block (the sunlight-exposed edges were generously removed under laboratory conditions). Two additional samples were collected with steel tubes from the Baierbrunn outcrop in an overlying layer located approximately 100 m to the south (Fig. 3a; BB1: VLL-0645-L and VLL-0648-L). Luminescence dating uses minerals as dosimeters to calculate the last sunlight exposure of sediment samples. Here, single grains of potassium-rich feldspar are used. One of the principal challenges of luminescence dating of water-lain sediments

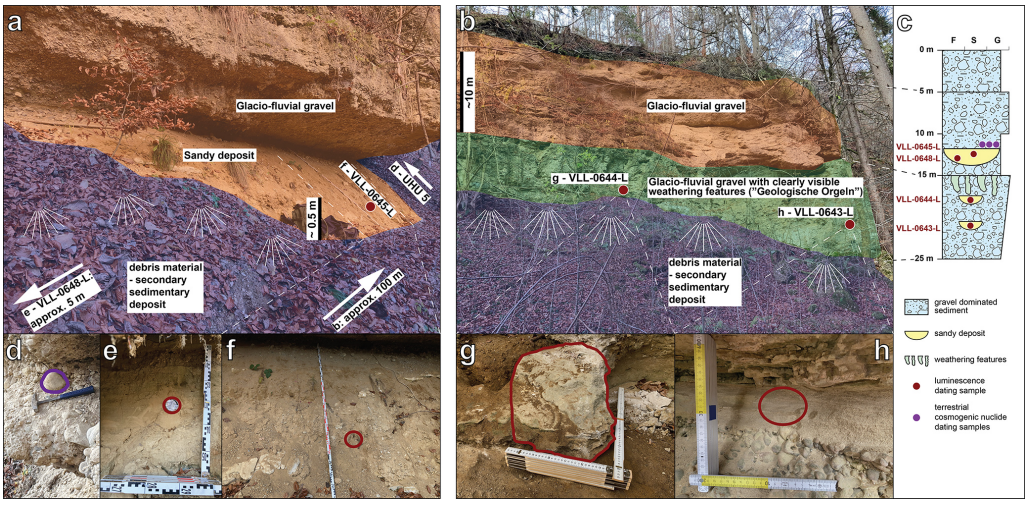

Figure 3. **(a)** (BB1) and **(b)** (BB2): overview of the sensu lato outcrop Baierbrunn ("Münchner Klettergarten") with the two visible main sections shaded in green and orange. Debris material is shaded in blue. The outcrop was accessed on two locations approximately 100 m apart. Sensu stricto only **(b)** shows the "Münchener Klettergarten", while **(a)** shows an adjacent outcrop to the south. **(c)** Simplified lithological column with the sampling locations indicated by dark-red circles. Quartz cobble UHU 5 **(d)**, sampled from glaciofluvial gravel overlying a larger channel-like sandy deposit for terrestrial cosmogenic nuclide dating; samples UHU 6 and UHU 7 were taken from the same stratigraphic horizon. VLL-0648-L **(e)** and VLL-0645-L **(f)** were taken from a larger channel-like sandy deposit. VLL-0644-L **(g)** and VLL-0643-L **(h)** were taken from sand layers within the glaciofluvial gravel. For a close-up of the weathering features ("Geologische Orgeln"), we refer to the Supplement (Fig. S2).

is the incomplete resetting of the signal due to insufficient sunlight exposure. Measurements conducted on single grains can isolate the well-bleached grain population to derive the depositional age (Duller, 2008). Firla et al. (2024a) investigated complex single-grain equivalent dose distributions from potassium-rich feldspar to overcome challenges associated with the dating of poorly bleached water-lain sediments, and they present a comprehensive approach to successfully derive ages from such sedimentary environments. All details on sample preparation, experimental set-up, compilation and evaluation of equivalent dose distributions, application of statistical age models and age calculation are provided in Firla et al. (2024a). Measurements were conducted at the Vienna Laboratory for Luminescence dating (VLL).

Application of the approach of Firla et al. (2024a) requires similar sample characteristics. This includes reliability of the applied $pIRIR_{225}$ (Buylaert et al., 2009; Reimann et al., 2012; Rades et al., 2018) single aliquot regenerative (SAR) dose protocol, fading properties, signal saturation levels and applicability of statistical age models. To test the reliability of the applied $pIRIR_{225}$ protocol (Firla et al., 2024a), we conducted dose recovery experiments on multiple samples using a given dose within the expected dose range, as derived from initial range finder tests. Samples showed bright luminescence signals, and dose response curves were fitted to a single saturating exponential function (Fig. 4). The average dose recovery for samples VLL-0553-L, VLL-0558-L and VLL-0645-L was 0.99 ± 0.01.

When using feldspar as a dosimeter, the potential occurrence of athermal signal loss (anomalous fading) must be considered, otherwise the depositional age would be underestimated. Firla et al. (2024a) discussed this topic in detail. Using their approach, we conducted fading test measurements (Auclair et al., 2003) on four samples (VLL-0553-L, VLL-0558-L, VLL-0560-L and VLL-0644-L). Results are in line with findings from Firla et al. (2024a). Individual g values show large scatter including negative g values resulting in an average g values of $\sim 1\,\%$ for the $pIRIR_{225}$ signal. For this calculation, negative values were excluded because negative fading is physically impossible. Had they been included, the resulting average g value would have been significantly lower. Previous research often considers fading rates of up to 1.5 % as laboratory artefacts, summarised by Lomax et al. (2022). Additionally, there is no general consensus on how to deal with such low fading rates (compare discussion of Firla et al., 2024a). To better characterise the samples, we conducted a range finder test using the $pIRIR_{290}$ signal (Thiel et al., 2011; Kars et al., 2012; Buylaert et al., 2012), which has been shown to exhibit even lower to no fading rates compared to the $pIRIR_{225}$ signal. Although the $pIRIR_{290}$ protocol is not suitable for age measurements because the yield of acceptable equivalent dose values is too low, we were able to obtain equivalent dose values for VLL-0644-L in the same range as for the $pIRIR_{225}$ signal (Fig. S5). Because of that, we conclude that there is no significant fading in the $pIRIR_{225}$, hence no fading correction was applied.

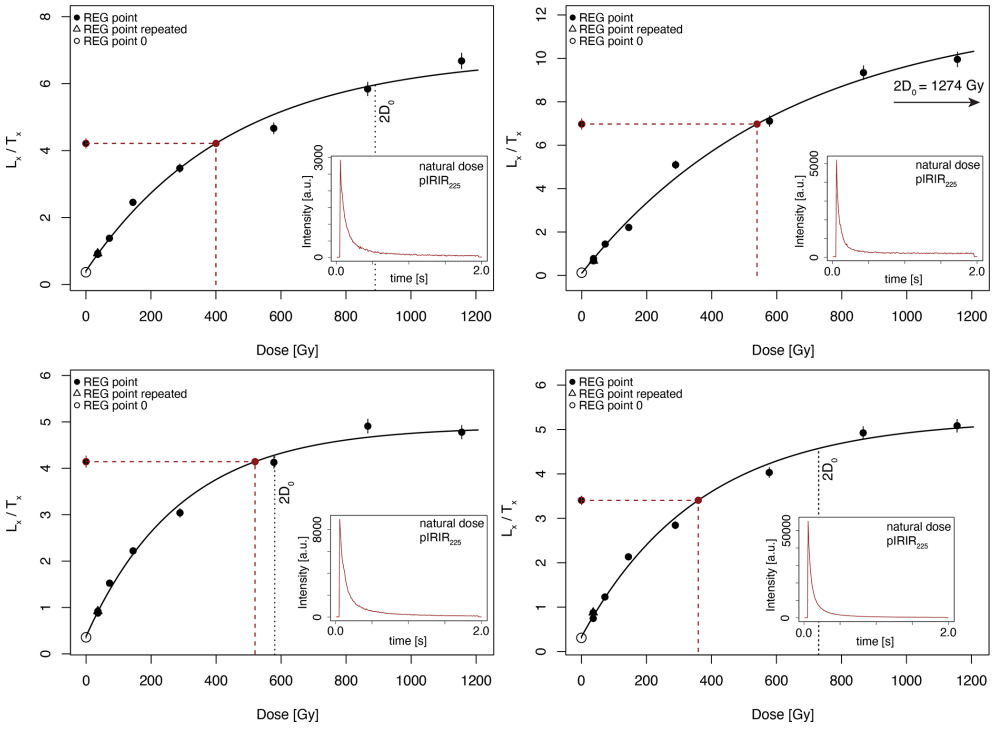

Figure 4. Exemplary single-grain dose response curves from VLL-0553-L, with the highest regenerated dose being ∼ 1150 Gy. Inset: shine-down curve showing a bright luminescence signal emitted by a single K-Fs grain after $pIRIR_{225}$ stimulation (natural dose).

The results from the $pIRIR_{290}$ test measurements also show that VLL-0644-L is not in field saturation. Whenever operating close to saturation, extra caution is advised. Wintle and Murray (2006) introduced the $2D_0$ parameter, which marks the 86 % saturation point on the exponential dose-response curve. VLL-0553-L, VLL-0555-L and VLL-0557-L exhibited equivalent dose distributions where ∼ 63 % of the equivalent dose values were below the $2D_0$ threshold and span over a comparable equivalent dose range (Fig. S4) compared to the equivalent dose values above $2D_0$. Firla et al. (2024a) argued for the inclusion of the equivalent dose values above $2D_0$ for the most reliable average equivalent doses, therefore all equivalent dose values (below and above the $2D_0$ threshold) are used for age calculation. In addition, the shape of the equivalent dose distribution can be used to infer the bleaching characteristics of the samples (Firla et al., 2024a).

Details on the applicability of statistical age models are provided in Sect. 4.3.

The content of radionuclides (^{238}U, ^{232}Th, ^{40}K – Table 1), contributing to the overall dose rate, were measured at the University of Bern, Switzerland, using a high-resolution low-level gamma spectrometer (Preusser and Kasper, 2001; well-type Ge detector, Canberra GCW2543-7500SL). Measurements were conducted over 2–3 d per sample using Marinelli beakers containing 750 g of material after storage over at least 1 month to reach secondary secular Rn equilibrium. The dose rate calculation followed the approach described in Firla et al. (2024a). The contribution of cosmic radiation to the total dose rate was considered using the burial depth, altitude, latitude and longitude of the samples (Prescott and Hutton, 1994; Prescott and Stephan, 1982). From the sedimentary context, we expect instant burial after deposition. However, we cannot exclude phases of erosion and redeposition. Because of that, the cosmic dose rate was assigned an uncertainty of ±10 %. However, given the burial depth of the samples, the contribution of the cosmic dose rate to the overall dose rate is very low (the shallowest sample VLL-0645-L has a cosmic dose rate contribution of approximately 3 %). For age calculation, an alpha attenuation factor of 0.07 ± 0.02 (Klasen, 2008) and an internal potassium content of 12.5 ± 0.5 % (Huntley and Baril, 1997) was used. Given the assumption of instant burial and taking into account today's hydrological conditions, we assume the samples have been at least close to water saturation for the majority of the burial period. Therefore, an average estimated water content of 25 ± 10 % was assumed to reflect these conditions.

3.3 Palynological screening

Ten samples were taken from unit A of the drill core for micro-botanical analysis in a 5–10 m interval. Analysis was conducted at the CNR-IGAG Laboratory of Palynology and Paleoecology in Milan, Italy (Pini and Bertuletti, 2023).

Table 1. Overview of the single-grain luminescence dating results. Bold ages are considered as reliable and the italicised age as unreliable.

	Dose rate results					$pIRIR_{225}$ measurement results			
Sample ID	Depth (m)	^{40}K ($Bq\,kg^{-1}$)	^{238}U ($Bq\,kg^{-1}$)	^{232}Th ($Bq\,kg^{-1}$)	DR[a] ($Gy\,ka^{-1}$)	n[b]	σ_b^c (%)	MAM-3 D_e^d (Gy)	Age[e] (ka)
Schäftlarn									
VLL-0560-L	91.30	25.4 ± 0.7	21.7 ± 3.2	1.5 ± 0.2	1.3 ± 0.1	131	25	305 ± 7	**240 ± 16**
VLL-0559-L	98.00	33.3 ± 1.0	23.3 ± 2.2	2.1 ± 0.2	1.3 ± 0.1	107	23	320 ± 8	**244 ± 17**
VLL-0558-L	102.85	38.9 ± 0.7	18.3 ± 1.7	2.8 ± 0.1	1.3 ± 0.1	133	32	332 ± 11	**258 ± 18**
VLL-0557-L	189.65	221.4 ± 4.7	22.6 ± 5.0	20.4 ± 0.4	2.0 ± 0.2	96	25	584 ± 17	**291 ± 24**
VLL-0556-L	191.70	204.0 ± 4.0	21.5 ± 6.0	17.2 ± 0.4	1.8 ± 0.1	90	30	542 ± 19	**294 ± 24**
VLL-0555-L	193.35	189.9 ± 5.4	12.9 ± 3.9	14.2 ± 0.4	1.8 ± 0.1	104	36	450 ± 23	**251 ± 23**
VLL-0554-L	197.10	191.7 ± 2.5	19.1 ± 1.9	15.3 ± 0.4	1.8 ± 0.1	82	29	558 ± 17	**312 ± 25**
VLL-0553-L	198.30	188.2 ± 2.8	19.9 ± 1.1	14.4 ± 0.3	1.8 ± 0.1	88	30	561 ± 17	**315 ± 25**
Baierbrunn									
VLL-0645-L	12.00	173.9 ± 3.6	23.1 ± 4.3	19.8 ± 0.3	1.9 ± 0.1	101	37	349 ± 15	**183 ± 16**
VLL-0648-L	13.00	177.2 ± 4.2	34.0 ± 7.0	22.7 ± 0.9	2.0 ± 0.2	164	30	385 ± 15	**191 ± 17**
VLL-0644-L	18.00	108.1 ± 2.1	12.9 ± 1.1	9.2 ± 0.2	1.4 ± 0.1	82	38	361 ± 17	**258 ± 21**
VLL-0643-L	21.00	20.8 ± 0.8	15.6 ± 2.7	1.2 ± 0.2	1.2 ± 0.1	49	65	109 ± 12	*> 92 ± 11*[f]

[a] Overall effective dose rate caused by cosmogenic and environmental ionising radiation. [b] Number of grains passing SAR rejection and low outlier rejection criteria (Firla et al., 2024a). [c] Overdispersion derived from Central Age Model (CAM) calculations. [d] Bootstrapped MAM-3 (Cunningham and Wallinga, 2012) equivalent dose calculated using the R luminescence package (Kreutzer et al., 2012). Overdispersion: 30 ± 10 %. [e] Age calculated using the ADELE software (Kulig, 2005). [f] Considered as minimum age due to contamination with bleached grains during sampling.

Samples were weighed and their volume estimated, and Lycopodium tablets were added prior to the chemical treatment to allow for the calculation of pollen and pollen-slide charcoal concentrations (Stockmarr, 1971).

3.4 Gravel petrographic screening

To identify potential variations in provenance, seven samples were collected for clast petrographic analysis from half-core sections of the gravel-dominated unit B of the Schäftlarn core (115.5–4 m, Fig. 5). Each sample was taken from section lengths ranging from 15 to 50 cm. The material was wet-sieved and the medium to coarse gravel fraction (6.3–63 mm) was macroscopically analysed (number of analysed clasts per sample range from 109 to 197). Following the classification established by Dreesbach (1986) for the Isar-Loisach Glacier region, the lithologies were divided into four groups: (1) limestone and marl, (2) dolomite, (3) other sedimentary rocks (sandstone, calcarenite, radiolarite) and (4) crystalline lithology (vein quartz, gneiss, amphibolite, quartzite and mica schist).

3.5 Geophysical investigation

In autumn 2023, a reflection seismic investigation was carried out on three profiles (Figs. 1c and S6). First, a north–south profile aligned in extension of the drill site (SL-1). Second, an east–west profile cuts the north–south profile just north of the drill site (SL-2). Lastly, a profile aligned parallel to the first north–south profile shifted to the east, located in the recent Isar Valley incision (SL-3). The combination of the drill core information and the geophysical survey allow us to trace sedimentary units from the drill core into three dimensions. The drill core additionally provides a "ground-truthing" cross-check for the geophysical profiles. The seismic reflection profiles were acquired using P-waves as well as an SH-wave configuration (Burschil, 2024). A first interpretation of the geophysical measurement results is presented here.

3.6 Terrestrial cosmogenic nuclide burial age dating

The combination of the cosmogenic radionuclides (CRNs) ^{10}Be and ^{26}Al, produced in quartz by secondary cosmic rays, is often used to identify the time of deposition of a sediment body (e.g. Balco and Rovey, 2008; Erlanger et al., 2012). This method can resolve depositional events in the time range between 100 ka and ca. 5 Ma (e.g. Granger, 2006) and is therefore ideally combined to luminescence methods to resolve the depositional history of Pliocene and Quaternary deposits. Both CRNs are produced at the surface at a different rate as well as by different production pathways that depend on depth (Heisinger et al., 2002a, b). The $^{26}Al/^{10}Be$ production rate ratio at the surface remains roughly constant at 6.7 ± 0.6 (for spallation, see Fenton et al., 2022). The main prerequisite to obtain reliable CRN burial ages is that the surface was exposed long enough to accumulate CRNs in measurable amounts and that the surface ratio was retained before the sediment was buried at the sample location after

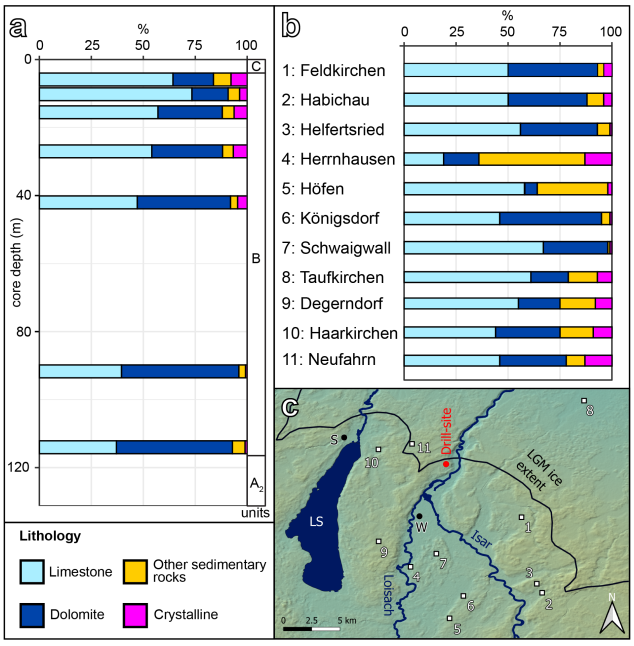

Figure 5. **(a)** Gravel petrographic screening results from unit B of the 5068_3_A Schäftlarn core. A significant increase in crystalline content from the basal two samples (∼ 0.9 %) to the top five samples (∼ 5.8 %) can be observed, as well as a shift in the ratio of limestone to dolomite (top five samples: ∼ 2.4, bottom two samples: ∼ 0.7). **(b)** Gravel petrographic results from last glacial glaciofluvial deposits in the Wolfratshausen region (Dreesbach, 1985). The crystalline content (∼ 5.7 %) and limestone to dolomite ratio (∼ 2.4) are similar/identical to the top five screening samples from 5068_3_A Schäftlarn. **(c)** Map of gravel petrographic analysis sites (LS = Lake Starnberg, S = Starnberg, W = Wolfratshausen).

transport without prolonged intermediate storage (Granger, 2006, 2014; Ruszkiczay-Rüdiger et al., 2025). In the source area, the concentration of cosmogenic nuclides is inversely coupled to the denudation rate (Ruszkiczay-Rüdiger et al., 2025).

Once buried, CRN production decreases or even stops if the burial depth is sufficient (below 30 m), and subsequent radioactive decay reduces the concentration of CRNs in the sample. Due to the different half-lives of ^{10}Be (1.387 ± 0.012 Ma; Chmeleff et al., 2010; Korschinek et al., 2010) and ^{26}Al (705 ± 17 ka; Nishiizumi, 2004), the initial (surface) ratio decreases with increasing burial time. This decrease is used to determine the burial duration of the sample (Granger, 2014).

In (glacio)fluvial settings such as the Klettergarten outcrop, the production of CRNs after burial is to be expected if the sampled sediment bodies are not covered by sufficient overburden. Post-burial production depends on the thickness and the erosion rate on site and must be accounted for by the selection of a suitable sampling strategy and method for age calculation (Ruszkiczay-Rüdiger et al., 2025). The sampling strategy was to retrieve cobbles from one depositional event at the same depth (and thus the same post-burial production) for isochron burial dating (Balco and Rovey, 2008; Erlanger et al., 2012) and isochron inverse modelling (Braucher et al., 2009) to obtain the time of gravel deposition. Both methods are applicable for settings where post-burial production is likely. The isochron method (Erlanger et al., 2012) is appropriate in settings with changing overburden (such as loess cover) because all cobbles are similarly affected. The inverse model (Braucher et al., 2009) is useful to obtain not only the age but also information on the on-site and catchment denudation rate, but a constant depth since deposition has to be assumed (Ruszkiczay-Rüdiger et al., 2025).

Laboratory procedures for CRN extraction at the BOKU CRN preparation laboratory involve physical (such as crushing, sieving and magnetic separation) and chemical steps (leaching to remove meteoric ^{10}Be) to isolate quartz. Next, purified quartz is dissolved in HF-HNO_3, and all elements except Al and Be are removed by pH selective precipitation and ion exchange. Al and Be are separated by ion exchange, dried, mixed with an Nb (for Al) and Fe (for Be) binder, and measured by accelerator mass spectrometry (AMS, VERA, Vienna Environmental Research Accelerator, Physics, University of Vienna). To calculate the ^{26}Al concentrations from AMS ratios, the total Al mass (Table 2) was calculated from ICP-OES (Institute of Forest Ecology, BOKU University) measurements of sample aliquots. One full process blank was processed with the samples. Technical details beyond this short summary can be found in a laboratory comparison study between the CRN preparation laboratories in Budapest and BOKU Vienna (Ruszkiczay-Rüdiger et al., 2021).

4 Results

4.1 Core description

The 5068_3_A Schäftlarn drill core is 198.8 m long. The succession consists of 15 different sedimentological lithotypes (Fig. 2). The lithotypes identified are defined in detail in Schaller et al. (2023) and Schuster et al. (2024). The drill core can be divided into ∼ 83 m of fine-grained sediments at the base, followed by ∼ 111 m of coarse-grained sediments, and on top ∼ 4 m of diamictic sediments. The Upper Freshwater Molasse bedrock was not reached, but remnants of a basal diamicton could be recovered. The recovered succession was grouped into three main lithostratigraphic units based on the identified lithotypes.

4.1.1 Lithostratigraphic unit A: 198.8–115.5 m b.s.

Basal unit A consists mainly of silt/clay sediments. It can be further divided into subunit A1 (198.8–183.4 m) and A2 (183.4–115.5 m). The silt/clay section of A1 are interbedded with sandy layers (Fig. 6). Some of these layers are non-horizontally bedded. Unit A2 lacks sandy layers and is dominated massive silt/clay deposits. Outsized gravel clasts are

Table 2. CRN analytical data of samples. All samples were processed at the laboratory for CRN extraction (Institute of Applied Geology, BOKU Vienna). Accelerator mass spectrometry (AMS) measurements of the $^{26}Al/^{27}Al$ (Lachner et al., 2021) and $^{10}Be/^{9}Be$ (Steier et al., 2019) were analysed at the Vienna Environmental Research Accelerator (VERA; Faculty of Physics, Isotope Physics, University of Vienna) against secondary standards. For aluminium, SMD-Al-11 ($(9.66 \pm 0.14) \times 10^{-12}$, Rugel et al., 2016) was used. For beryllium, all samples were normalised to SMD-Be-12 ($(1.704 \pm 0.030) \times 10^{-12}$, Rugel et al., 2016). A process blank (with a ratio of $(4.7 \pm 0.54) \times 10^{-15}$ for Be and $(3.92 \pm 0.79) \times 10^{-15}$ for Al) was processed. Reported uncertainties include the AMS measurement, uncertainty of the standard materials, the ICP-OES Al measurement (Institute of Forest Ecology, BOKU Vienna) and 2 % error on weighing of samples and carriers. The percent of blank correction (bc) for ^{26}Al and ^{10}Be are listed.

Sample number	Quartz dissolved	$^{10}Be/^{9}Be \pm 1\sigma$ analytical unc.	Be from carrier	$Conc^{10}Be \pm 1\sigma$ analytical unc.	^{10}Be bc	Al total (spike + native)	$^{26}Al/^{27}Al \pm 1\sigma$ analytical unc.	$Conc^{26}Al \pm 1\sigma$ analytical unc.	^{26}Al bc	$^{26}Al/^{10}Be$
	(g)		(µg)	(atoms per g quartz)	(%)	(mg)		(10^3 atoms per g quartz)	(%)	
UHU 5B	45.3734	$13.37 \pm 0.58 \times 10^{-14}$	253.2885	48.120 ± 2.379	3.6	2.93202	$16.74 \times 10^{-14} \pm 0.79$	33.975 ± 2.341	2.1	0.71
UHU 6B	18.2711	$5.35 \pm 0.20 \times 10^{-14}$	253.933	45.321 ± 2.155	9.6	10.71285	$3.85 \times 10^{-14} \pm 0.30$	201.500 ± 18.730	0.8	4.45
UHU 7B	49.5856	$1.98 \pm 0.17 \times 10^{-14}$	253.933	5.167 ± 630	31.1	2.30092	$7.327 \times 10^{-14} \pm 0.40$	12.511 ± 930	5.0	2.42

present in unit A1 and in the lower part of unit A2. The transition from unit A1 to A2 is associated with a minor decrease in wet bulk density and magnetic susceptibility but with an increase in natural gamma radiation and average grain size. The organic matter content shows small variations within a comparatively low average value (0.4 %–1.4 %). The carbonate content is comparatively consistent over the whole length of unit A (∼ 55 %). It is also within the range of the source bedrock found in the glacier catchment area (i.e. mainly Molasse and Northern Calcareous Alps). The contact between unit A and unit B is sharp, with an abrupt colour change in the fine-grained section from blueish-grey to reddish-brown.

4.1.2 Lithostratigraphic unit B: 115.5–4 m b.s.

Unit B is dominated by gravel deposits (Fig. 6). The gravelly sediments at the transition from unit A to unit B are fully cemented over the whole width of the core. This transition is clearly visible in the magnetic susceptibility and natural gamma-radiation measurements (Fig. 2). Astonishingly, the succession retrieved is comparatively homogeneous over the whole length of unit B, with only minor changes in dominant clast size. The grain size in the gravel matrix increases slightly from a more sand-dominated matrix at the base of unit B to a more silt-dominated matrix at the top. Some ∼ 20 cm large sand layers are present between 112 and 91 m. A singular silt-dominated layer is present at 60.5 m. The wet bulk density and the natural gamma radiation show consistent values for the investigated sections of unit B. Magnetic susceptibility values vary in the section from 70 to 4 m. From 115.5 to 70 m, magnetic susceptibility exhibits a lower baseline, with some more pronounced peaks.

Gravel petrography revealed a difference in the crystalline content between the basal two samples and the top five samples (Fig. 5). The basal two samples show a depleted crystalline content of 0.8 % and 1.0 %, similar to gravel petrography results from Jerz et al. (1987) that were associated with the Mindel glaciation. The top five samples contain a higher number of crystalline clasts (3.7 %–7.8 %) similar to values reported in Dreesbach (1985, 1986) that were associated with younger glaciations (Fig. 5). In addition, a shift in the ratio of limestone to dolomite was observed between the top five samples (∼ 2.4) and the bottom two samples (∼ 0.7). Our results from the top five samples are in excellent agreement with Dreesbach (1985) (∼ 2.4), also associated with the last glaciation.

4.1.3 Lithostratigraphic unit C: 4–0 m b.s.

The topmost unit consists mainly of diamictic sediments. A gradual transition from clast-supported to matrix-supported diamicton can be observed (Fig. 6). The top 1.3 m shows clear indications of soil development, and the top 0.3 m can be described as ploughed soil horizon.

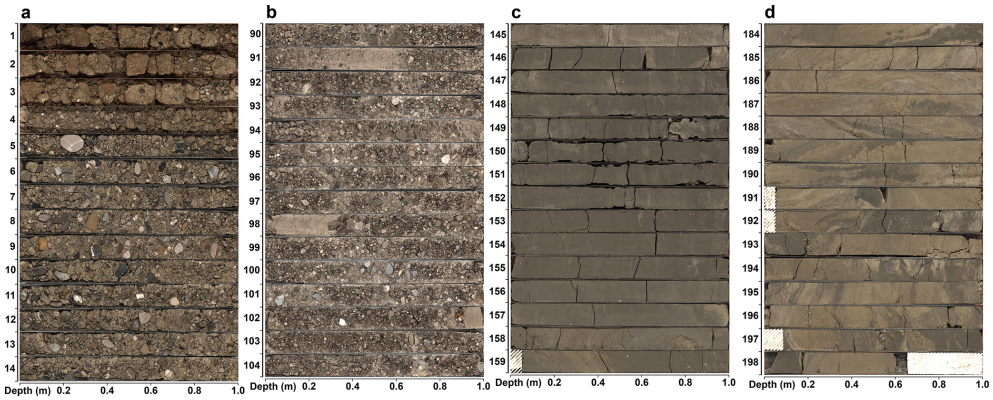

Figure 6. Line scan overview of selected core sections (x axis: depth in section, y axis: top depth of section in core, white hatched sections: core loss): **(a)** transition from diamictic unit C to gravel-dominated unit B, **(b)** sandy gravel sections of unit B, **(c)** silt/clay-dominated sections at the top of unit A2 and **(d)** silt/clay sections with partially convoluted sand layers.

4.2 Outcrop Baierbrunn – "Münchner Klettergarten"

The outcrop consists of gravel-dominated glaciofluvial deposits (Fig. 3) and is located on a scarp eroded by the river Isar. The outcrop was accessed at two locations (Fig. 3a: BB1, Fig. 3b: BB2). It can be divided into four horizontal sections. The basal part of the section is constituted by cemented gravel-dominated deposits showing a coarsening-up trend (15–25 m). This section is characterised by weathering features at the intersection between the overlying section and isolated sand layers. Following that are finer cemented gravel-dominated sediments (10–15 m). This section can be traced approximately 100 m to the south, where a sandy deposit with a channel-like morphology is overlain by glaciofluvial sediments (Fig. 3a – BB1). The overlying section (5–10 m) is made up out of slightly coarser cemented gravel deposits. The top section (0–5 m) consists of uncemented gravels. Downslope of the outcrop, towards the river Isar, debris from slope failures is ubiquitous, providing evidence of the past mass movement dynamic of the Isar Valley. To emphasise this dynamic, following the sampling conducted in December 2022, the upright front face of the outcrop collapsed during the summer of 2023 and is no longer accessible.

4.3 Luminescence dating

All samples showed a right-skewed equivalent dose (D_e) distribution (Fig. 7). Additionally, most samples exhibited high overdispersion values. These sample characteristics are indicative of incompletely bleached sediments common to glacially associated deposits. Because of the occurrence of LOVED (Low Outlier Value Equivalent Dose) grains, the correction approach of Firla et al. (2024a) was applied. To calculate equivalent doses representative of the depositional event, a statistical Minimum Age Model approach is required. In such approaches, the determination of a robust σ_b value is essential. Unfortunately, this cannot be derived from a well-bleached sample because all samples are poorly bleached. Firla et al. (2024a) presented an overdispersion value for a well-bleached sample of 23 % from a similar depositional environment.

Consequently, we applied the bootstrapped (Cunningham and Wallinga, 2012) three parameter Minimum Age Model (MAM-3; Galbraith et al., 1999) for the average equivalent dose calculation of all samples, using a σ_b of 30 ± 10 % as the threshold.

An overview of the luminescence dating results is given in Table 1. Average cluster ages for 5068_3_A were calculated using the Central Age Model (CAM) (Galbraith et al., 1999). The basal age cluster of the 5068_3_A core can be attributed to early MIS 8 (294 ± 11 ka, Fig. 8). This age cluster consists of five ages. Four ages in this cluster agree within uncertainty. VLL-0555-L is considered a low outlier because it agrees with only two other samples in the age cluster within uncertainty. It shows an age agreeing with late MIS 8. The underestimation of VLL-0555-L is likely caused by difficulties in fitting a normal distribution to the leading edge after Firla et al. (2024a) and therefore potentially not dismissing all underestimating LOVED grains. No samples were taken from unit A2 because of a lack of suitable material (i.e. no sand layers in clay/silt-dominated sections). The age cluster at the bottom section of unit B can be attributed to late MIS 8 (247 ± 10 ka, Fig. 8). Similar to the basal cluster, the samples in the top cluster agree within uncertainty. Similar to unit A2, no additional samples could be obtained from the top section of unit B because of a lack of suitable sediments (i.e. no sand layers in gravel-dominated sections).

Results from the lower section of the Baierbrunn outcrop suggest deposition in a similar time frame compared to the sample cluster in unit B of core 5068_3_A (late MIS 8). Results from the upper section suggests deposition at a later stage (MIS 6) (Fig. 9). VLL-0644-L (258 ± 21 ka), VLL-0645-L (183 ± 16 ka) and VLL-0648-L (191 ± 17 ka) represent the depositional age because here the most likely well-

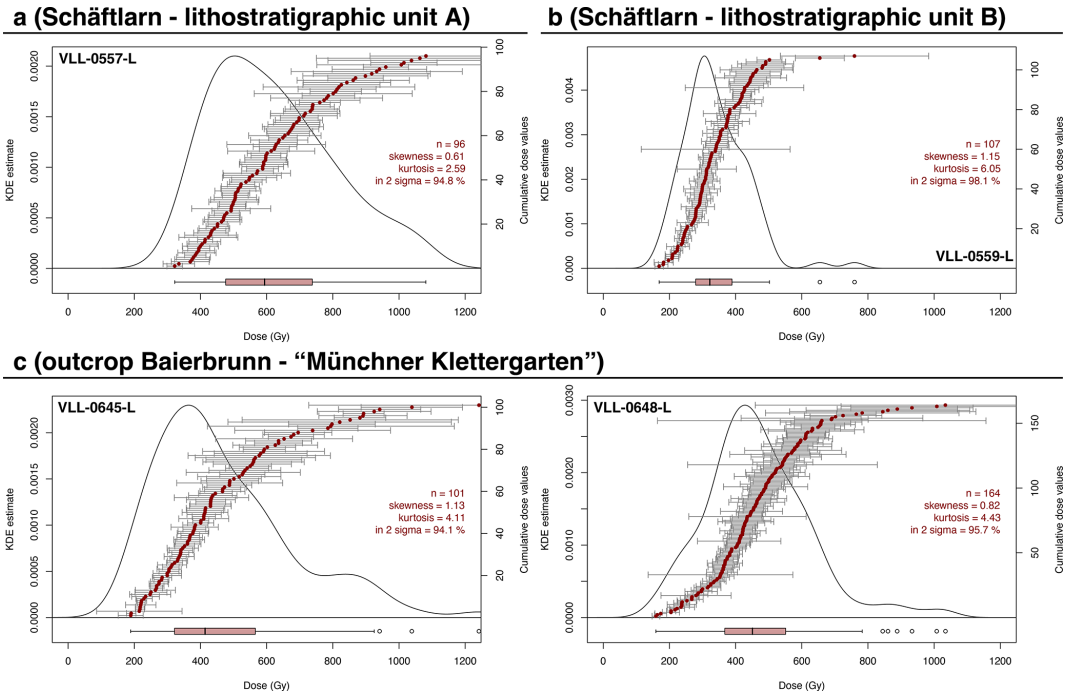

Figure 7. **(a)** KDE plot showing the exemplary single-grain equivalent dose distribution of sample VLL-0557-L from the 5068_3_A SCHA unit A age cluster. **(b)** KDE plot showing the exemplary single-grain equivalent dose distribution of sample VLL-0559-L from the 5058_3_A SCHA unit B age cluster. **(c)** KDE plots showing exemplary single-grain equivalent dose distributions of VLL-0645-L and VLL-0648-L from the Baierbrunn outcrop. For KDE plots from all measured samples, please refer to the supplementary material (Fig. S3).

bleached population could be isolated (Fig. 9). For VLL-0643-L, it was not possible to calculate a reliable depositional age, because of issues during sampling and contamination with light exposed grains that could not be removed by preparation techniques or statistical approaches. Therefore, the age calculated for VLL-0643-L must be considered as a minimum estimate ($> 92 \pm 11$ ka). What can be said with confidence is that there is a significant age difference between the upper two samples and the lower samples at the Baierbrunn outcrop.

4.4 Palynological screening

The analysis yielded a low amount of moderately well-preserved Quaternary palynomorphs. Poorly preserved Neogene up to Early Pleistocene palynomorphs and the remains of marine organisms (dinocyst, foraminifera organic lining) suggest reworking of Molasse bedrock and older Quaternary deposits (Streel and Bless, 1980; Batten, 1991). The pollen spectra, dominated by reworked particles, does not allow for any reliable conclusion about the vegetation cover during the deposition of unit A.

4.5 Geophysical investigation

The three seismic profiles provide insights into the sedimentary composition of the Schäftlarn overdeepening (Fig. 10). The seismic profiles can be structurally divided by tracing major reflectors. We identify five different seismic facies, which we interpret as the following lithologies:

1. Gravel-dominated sediments with weaker cementation,
2. Gravel-dominated sediments with stronger cementation,
3. Fine-grained basin sediments,
4. Basal diamictons and/or reworked Molasse bedrock,
5. Molasse bedrock sediments.

The last two facies cannot always be unequivocally differentiated, but both facies denote more or less the base of the overdeepened structure. In the northern part, profile SL-1 revealed a covering gravel layer at the top that splits into a section with stronger cementation and a section with a lesser degree of cementation, followed by fine-grained basin sediments. Below the basin sediments, a basal glacial diamicton is visible as a concave shape. The Molasse bedrock is situated below the diamicton, which cannot be distinguished with any certainty. To the south, we interpret a second older basin generation that is crosscut by the younger basin generation in the north. On top of this older basin, the covering gravels are thicker. This is due to part of the covering gravels being older and are as well cut by the younger basin generation. At the base of the older basin, the seismic facies

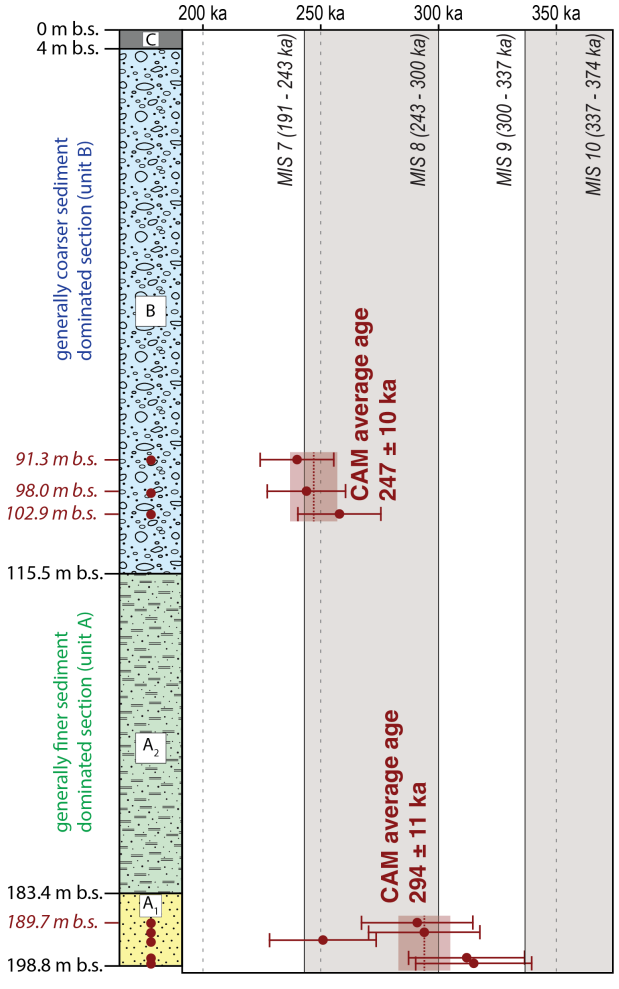

Figure 8. Luminescence dating age overview for core 5068_3_A Schäftlarn. Left: generalised lithological column, right: single-grain pIRIR$_{225}$ ages compared to the Marine Isotope Stages after Lisiecki and Raymo (2005). For detailed ages, see Table 1.

yield to a thick glacial diamicton. The seismic reflectors below, which we interpret as the bedrock contact, are not as clearly defined as the younger generation. The drill core was retrieved from the older basin. The east–west-oriented profile SL-2 shows the two basin generations as well. Following the basin fine-grained sediments are basal diamicton layers and below them the Molasse bedrock is again challenging to differentiate from the overlying diamicton. Similar to SL-1, two gravel layers with different thicknesses can be differentiated. On the easternmost edge of the profile, regular horizontal reflectors are interpreted as the Molasse bedrock positioned near the landscape surface in the recent Isar Valley. The seismic image exhibits a gap in resolution that is caused by the accessibility during data acquisition. In this section, we cannot observe the transition from the gravel-dominated layer to the Molasse bedrock but assume a continuous transition (Fig. 10). Profile SL-3 in the Isar Valley incision revealed a continuous horizontal reflection horizon near the landscape

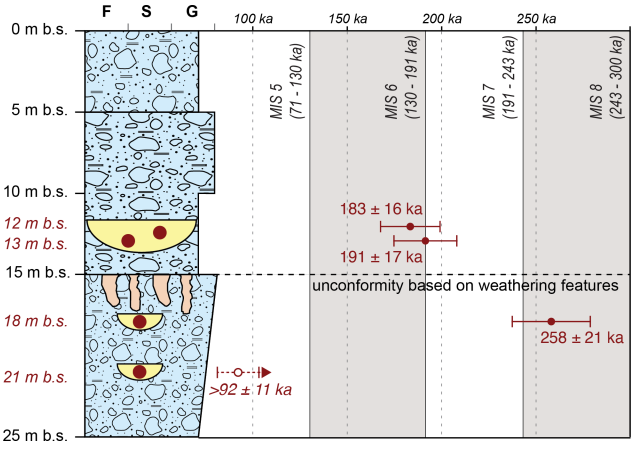

Figure 9. Luminescence dating age overview for the outcrop Baierbrunn ("Münchner Klettergarten"). Left: generalised lithological column from Fig. 3, right: pIRIR$_{225}$ ages compared to the Marine Isotope Stages, after Lisiecki and Raymo (2005). Filled circles indicate single-grain depositional ages (VLL-0645-L, VLL-0648-L, VLL-0644-L). The empty circle indicates a single-grain minimum age due to contamination with bleached grains during sampling (VLL-0643-L). A major unconformity is present at approximately the depth of the weathering features.

surface. This is interpreted as Molasse bedrock only covered by a few meters of Holocene alluvial sediments.

4.6 Terrestrial cosmogenic nuclide burial age dating

Results from CRN extraction of three samples ∼ 12 m below the surface gave ^{10}Be concentrations between ca 5000 and 50 000 atoms per g quartz and lower ^{26}Al concentrations of ca 12 000 to 200 000 atoms per g quartz (see Table 2).

Of all samples, UHU 7 has the lowest concentrations of CRN and consequently a high percentage of blank correction for both ^{26}Al (5 %) and ^{10}Be (ca 30 %). ^{10}Be concentrations are similar in samples UHU 5 and UHU 6, but their ^{26}Al is vastly different. Consequently, ^{26}Al/^{10}Be ratios range between 0.7 and 4.5 in all three samples.

Sample UHU 5 has a very low Al/Be ratio of 0.71, which indicates that much of the ^{26}Al was lost before deposition at the sampling site. In comparison, CRN concentrations of UHU 6 range at levels typically reported for Quaternary sediments derived from the Alps (Braumann et al., 2019; Ruszkiczay-Rüdiger et al., 2025). The concentrations were not converted into depositional ages because they disagree with the geologic setting and the luminescence ages (see also Sect. 5.2). In addition, the ^{10}Be and ^{26}Al concentrations do not correlate linearly, thus no isochron can be calculated from this dataset.

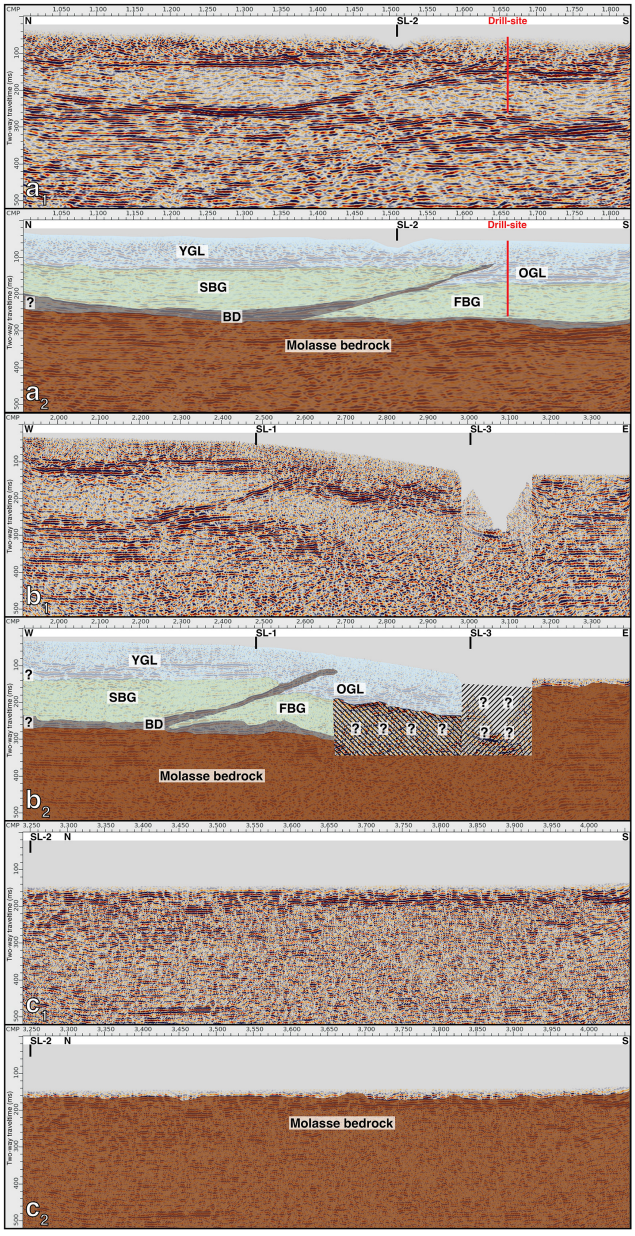

Figure 10. ($\mathbf{a_1}$): reflection seismic profile SL-1. ($\mathbf{a_2}$): reflection seismic profile SL-1 with added interpretation ($\mathbf{b_1}$): reflection seismic profile SL-2. ($\mathbf{b_2}$): reflection seismic profile SL-2 with added interpretation ($\mathbf{c_1}$): reflection seismic profile SL-3. ($\mathbf{c_2}$): reflection seismic profile SL-3 with added interpretation. Interpretation of seismic facies: brown – Molasse bedrock, grey – basal diamicton or reworked Molasse bedrock (BD), green – fine-grained deposits (MIS 8 first basin generation (FBG) and younger cutting second basin generation (SBG)), blue – gravel-dominated deposits (older gravel layer (OGL) and younger gravel layer (YGL)). Hatched areas and question marks denote areas of increased uncertainty.

5 Discussion

5.1 Reliability of the data

Serra et al. (2025) used the same measurement and age calculation approach (single-grain $pIRIR_{225}$) as presented here to analyse poorly bleached samples from a glaciofluvial outcrop (Finsterhennen) in the Northern Alpine Foreland of Switzerland. They found that the non-fading LOVED grain corrected age agreed with radiocarbon age control. Although the age range in Finsterhennen is younger, this provides further evidence in support of the reliability of the measurement and age calculation approach of Firla et al. (2024a), in addition to the arguments presented in Sects. 3.2 and 4.3.

Dosimetry results for the Schäftlarn unit B sample cluster and Baierbrunn samples VLL-0643-L and VLL-0644-L exhibit low values compared to other sites in the Northern Alpine Foreland (Salcher et al., 2015; Rades et al., 2018; Firla et al., 2024a).

Dosimetry results from Serra et al. (2025) provide similarly low dose-rate values. Their ages were calculated using these low dosimetry values and agree with independent age control. Klasen (2008) investigated the Munich gravel plain ("Münchner Schotterebene") with luminescence dating methods north of Baierbrunn. Some investigated sites showed similarly low dosimetry values. Finally, Bickel et al. (2015a) investigated glaciofluvial terrace sediments from the Northern Alpine Foreland. Some samples also show low activities, but the resulting ages are in good agreement with the overall stratigraphy and chronology. An analytical error was excluded as the high-resolution low-level gamma spectrometry results at the University of Bern are backed up by additional high-resolution low-level gamma spectrometry measurements at the University of Freiburg, Germany. At a closer look, low dosimetry values are caused by low content of ^{40}K and ^{232}Th. The ^{238}U content exhibits expected values. No disequilibrium in the U-series decay chain was detected. In addition, supporting spectral gamma ray wireline logging conducted in the drill hole revealed similar low ^{40}K decay and ^{232}Th decay chain activities for the entire length of unit B and thus support the double-checked gamma spectrometry results. It is highly unlikely that any post-sedimentary alteration in the ^{40}K decay and ^{232}Th decay chain activities can affect unit B homogeneously. We therefore conclude that the ^{40}K and ^{232}Th values, although conspicuously low, are reproducible and detectable in several locations. The uniqueness of these unusually low dosimetry results can be used as a geochemical parameter to correlate the glaciofluvial gravel section from 5068_3_A to the Baierbrunn outcrop. This adds additional evidence to the luminescence dating ages that the lower section of 5068_3_A SCHA sedimentary unit B is also present in the section below 15 m at the Baierbrunn outcrop.

If widened to a full investigation by including more sample, the palynological screening would not significantly change the resulting statement that the low content of Qua-

ternary pollen does not allow the reconstruction of the paleoenvironment. Because the topmost sample is comparable to the bottommost sample, we assume that the samples in between would show comparable pollen assemblages.

Similarly, we assume that, if widened to a full investigation, the petrographic screening would not significantly change the outcome, showing differences in the crystalline content between the top and the base of unit B.

5.2 Potential implications from the CRN dataset

CRN concentrations and ratios vary significantly for the three samples, and the $^{26}Al/^{10}Be$ ratios of all samples are very low. If these low ratios were to be converted to burial ages, they would indicate a high depositional age. This is in strong disagreement with luminescence ages from several locations in the outcrop and with the geological setting.

The reason for the offset between CRN data and information from luminescence could be the fast redeposition of material that was buried over a significant and prolonged time before reaching the sampling site. This is a realistic process in proglacial and glaciofluvial environments where significant amounts of sediment can be reworked during periods of high discharge.

Luminescence specifies an age of 180 ka for sand below the UHU cobbles (Fig. 3) sampled for CRN dating. Outstandingly low ^{26}Al in sample UHU 7 suggests that possibly even all ^{26}Al could have been produced after deposition. Using this assumption, we can integrate the luminescence age, the geographic parameters and a current depth of 12 m to estimate the surface denudation rate on site by applying the post-burial production test (Ruszkiczay-Rüdiger et al., 2025; their Eq. 2). This test was initially developed to identify outlier samples by using the depositional age, denudation rate on site and depth to calculate if the percent of ^{26}Al and ^{10}Be are in equilibrium. It can also be used to vary denudation rates to fit the depositional age and the measured ^{26}Al concentrations, to test if calculated rates range within geologic reasonable values. For sample UHU 7, the sample with the lowest concentrations, the denudation on site after deposition (assuming ^{26}Al was produced only after deposition) results in a denudation rate of 160 m Ma^{-1} (corresponding to $\sim$ 30 m in 180 ka). This denudation rate must be treated as the tentative maximum possible denudation after deposition under the assumption that the sample arrived without ^{26}Al and can be regarded as a maximum possible theoretical denudation rate at this location. The main argument for the presence of a significant cover are low $^{26}Al/^{10}Be$ ratios combined to low concentrations of both nuclides. If the surface was at constant depth over burial time, CRN production by muons would have driven the ratio towards higher values.

In summary, CRN concentrations could not be converted into depositional ages. Nonetheless, they can be used to speculate that the sampled UHU clasts were last exposed in the Pliocene or even before because of their low $^{26}Al/^{10}Be$ ratio and were buried deep, before fast redeposition at the current location.

5.3 New insights from the Isar-Loisach Glacier

The carbonate content of unit A is homogenous over the whole sedimentary succession, indicating a constant catchment area (Molasse and Northern Calcareous Alps) during deposition, without any major glacial transgression from the Inn Valley into the foreland. Influence from farther south would likely provide more crystalline sediments from the southern flank of the Inn Valley (Schuster et al., 2015). This is not recorded during MIS 8 in the Schäftlarn overdeepening.

A striking feature of unit B is the comparative homogeneity of its sediments. This might suggest that either the entire unit was potentially deposited in a steady state environment (i.e. with no significant change in proximity to the glacier front) over a potentially short time interval, or unit B represents a longer depositional time frame potentially spanning multiple MIS, originating from a similar sedimentary environment and lithological makeup (i.e. similar provenance and no significant difference in clast weathering). The second scenario would include the potential erosion of interglacial sediments.

Whether the overdeepening was excavated and subsequently filled during MIS 8 or the overdeepening was formed during a pre-MIS 8 glaciation and was re-excavated cannot be conclusively answered (Gegg and Preusser, 2023). The lack of any sediments older than MIS 8 suggest that if the overdeepened basin was formed before MIS 8, all sediments associated with previous glaciations were eroded and/or reworked, as is indicated by CRN and pollen data (Streel and Bless, 1980; Batten, 1991). This observation is not unique for the investigated overdeepened structure here but has been proposed for overdeepenings in the Alpine Foreland in general, where the morphological guiding (i.e. higher elevated mountain ranges constraining glacier flow direction) of the glacial basal erosion is not as pronounced. The Schäftlarn location is different from glacier proximal overdeepenings near valley outlets where every successive glaciation is forced into similar directions by the general valley patterns of high elevated mountain ranges (Gegg et al., 2025). In such a case, any glacier has a high likelihood of eroding previous glacially associated sediments or bedrock at the same position.

Comparing the results obtained here with the depositional age of other previously studied Northern Alpine Foreland overdeepened structures (Dehnert et al., 2012; Buechi et al., 2017; Mueller et al., 2024; Firla et al., 2024a, 2024b), it is noteworthy that the Schäftlarn overdeepening exhibits a different depositional chronology. Other overdeepened basins exhibit a similar sedimentary succession and depositional age (i.e. MIS 6 fine-grained basal infill and overlying coarser sediment associated with the last glaciation, except for the overdeepening presented in Dehnert et al. (2012) where the

MIS 6 fine-grained sediments are followed by another lake phase associated with the last glaciation). The succession presented here is different, with a thicker (115.5 m) coarser sedimentary unit at the top that is associated in the lower section with the same MIS 8. Hughes et al. (2020) termed MIS 8 as a "missing glaciation". They argue that MIS 8 was part of a comparatively weak glacial–interglacial cycle and that the configuration of controls on the global climate were different when compared to later glaciations, such as MIS 6. This discrepancy is underscored by the scarcity of MIS 8 terrestrial records in Europe, as opposed to the abundance of MIS 6 deposits. Known deposits that are attributed to MIS 8 in the Northern Alpine Foreland are the Meikirch record in northern Switzerland (Preusser et al., 2005) and the deposit presented here. The presence of MIS 8 sedimentary deposits has been documented along the margins of the Fennoscandian Ice Shield, extending from the United Kingdom to Belarus (Davies et al., 2012; Bates et al., 2014; Roskosch et al., 2014; White et al., 2017; Lauer and Weiss, 2018; Marks et al., 2020). Sediments from mountain glaciations in southern Europe during MIS 8 are recorded on the Iberian Peninsula, Italy and Montenegro (Fernández Mosquera et al., 2000; Hughes et al., 2011; Vidal et al., 2015; Giraudi and Giaccio, 2017). Such sites are uncommon, and their abundance stands in stark contrast to the prevalence of known MIS 6 deposits across Europe. It would be an arduous task to list all of these MIS 6 sites; therefore, here are a few examples from the Northern Alpine Foreland: Bickel et al. (2015a, b), Lowick et al. (2015), Salcher et al. (2015) and Rades et al. (2018). Furthermore, a considerable proportion of the MIS 8 sites previously mentioned also exhibit MIS 6 deposits.

5.4 Stratigraphical implications

The glacial series of Penck and Brückner (1909) is closely related to the terrace stratigraphy of Bavaria (Doppler et al., 2011). Terrace levels are interpreted as being the result of deposition linked to different glaciations, followed by (glacio)-fluvial erosion and with additional influence from tectonic uplift. These terraces occur in a reversed stratigraphic sequence (i.e. the oldest terrace deposits being at higher elevations compared to younger terraces being positioned at lower elevations). In contrast to this stratigraphy, which is valid in the Bavarian Alpine Foreland, the Munich gravel plain ("Münchner Schotterebene") follows a normal geological sequence with the oldest deposits at the base and the youngest deposits at the top (Jerz, 1993). The outcrop Baierbrunn is situated on the southern margin of the Munich gravel plain. The lower section of the outcrop, from which the bottom two luminescence dating samples were taken, has been proposed to be of Danubian or Günzian age (Jerz, 1993). Doppler et al. (2011) suggest that the Günz glaciation is older than MIS 12. The luminescence dating results presented here provide new insights into the depositional history. They disprove the hypothesis of deposition prior to MIS 12 (Donau or Günz) but reveal that deposition began during MIS 8 (Riss glaciation equalling MIS 6–10 according to Doppler et al., 2011). This would imply that the fourfold division of the Baierbrunn outcrop cannot be attributed to the four glaciations of Penck and Brückner (1909) but most likely represents different stages of the last two glacial cycles (Riss and Würm). Therefore, it can be suggested that the stratigraphical exception (Doppler et al., 2011) in the Bavarian Alpine Foreland – the Munich gravel plain – is younger than previously expected. However, the position of MIS 8 age deposits at the base of the outcrop (with likely younger deposits at the top divided by a weathering horizon) and the geophysical results from Schäftlarn presented here (with younger gravel deposits overlying older deposits) would reinforce the normal geological sequence of the Munich gravel plain ("Münchner Schotterebene"). We therefore suggest a threefold division of the glaciofluvial gravel deposits at the Baierbrunn outcrop – at the base MIS 8 deposits overlain by MIS 6 deposits with most likely last glacial deposits on top (MIS 2–5d). The last glacial deposits have been successfully identified north of Lake Starnberg by Reuther et al. (2011), and it seems conceivable that deposits of a similar time frame are present $\sim$ 10 km to the east at Baierbrunn. This division can be tentatively expanded to unit B of the Schäftlarn core. With MIS 8 at the base of unit B, overlain by potentially MIS 6 deposits (a high probability that MIS 6 deposits that have been identified at Baierbrunn are present in some quantity at Schäftlarn), further overlain by the last glacial sediments as suggested by the gravel clast petrography screening (Fig. 5) matching similar last glacial results in the vicinity (Dreesbach, 1985, 1986).

5.5 Landscape development

In the following subsection, the most probable landscape development scenario is given, based on the previously presented datasets (Fig. 11). As alluded to before, the first overdeepened basin was likely excavated during MIS 8. After the glacial erosion subsided and the glacier retreated, coarser sediments (potentially glacial till – Burschil et al., 2019) were deposited at the base of the MIS 8 basin. Following further glacial retreat, fine-grained sediment accumulated in the overdeepened structure. Following that, glaciofluvial sediments were deposited on top of the most likely glaciolacustrine section during late MIS 8. This glaciofluvial section can be traced farther north to the outcrop "Münchner Klettergarten" Baierbrunn, as similar dating results showed. After the first basin generation, a second basin generation developed after a new glacial advance. As the 5068_3 drill core is situated in the older basin, we can only say with absolute confidence that the other basin is younger due to the cross-cutting relationship. But we assume that this basin can be attributed to MIS 6 according to dating results from other investigated overdeepened basins (Dehnert et al., 2012; Buechi et al., 2017; Mueller et al., 2024; Firla et al., 2024a, 2024b). The glacial advance associated with the younger basin exca-

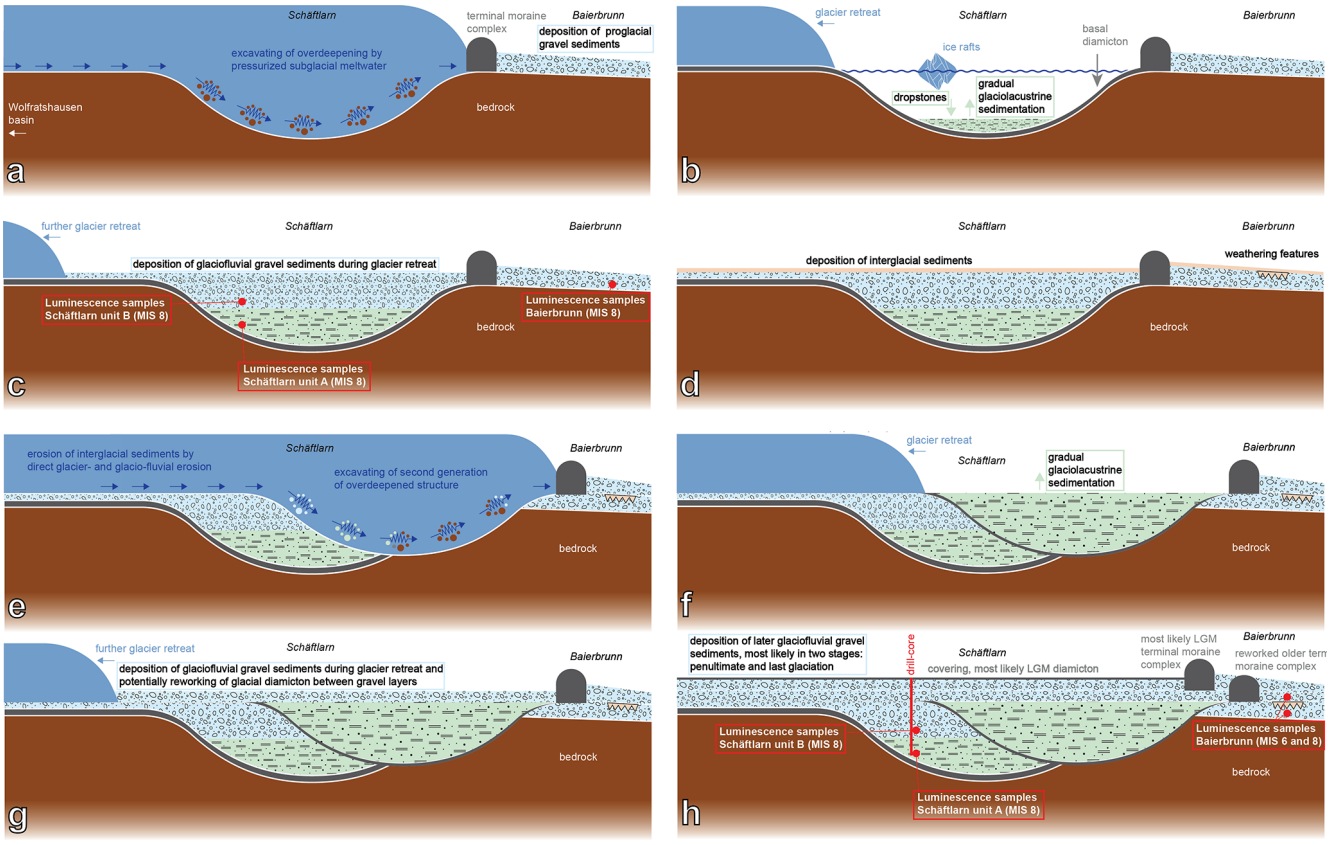

Figure 11. Schematic overview (not to scale) of the landscape development model of the Isar-Loisach foreland piedmont-style glacier lobe. Dark-blue = glacier, brown = Molasse bedrock, green = glaciolacustrine fine sediments, light-blue = glaciofluvial sediments, grey = diamicton sediments. **(a)** Initial excavation of first overdeepened basin and deposition of terminal moraine system. **(b)** Filling of overdeepening with fine-grained sediments after glacier retreat. **(c)** Deposition of glaciofluvial sediments overlying first-generation fine-grained sediments. **(d)** Deposition of interglacial sediments and development of weathering features at Baierbrunn. **(e)** Renewed glacial advance, erosion of interglacial deposits, excavation of older Pleistocene deposits and bedrock, and reworking of older terminal moraine system, creating a second cross-cutting, an overdeepened basin and a new terminal moraine system. **(f)** Filling of cross-cutting overdeepened basin with fine-grained sediments. **(g)** Covering of older glaciofluvial deposits on top of first basin and fine-grained infill of second basin by younger glaciofluvial deposits. **(h)** During the last glaciation, a renewed glacier advance deposited a new terminal moraine complex and reworked the older terminal moraine complex but did not excavate a new overdeepening. Younger glaciofluvial and diamicton sediments are most likely associated with the last glaciation.

vated parts of the MIS 8 sediments and/or Molasse bedrock. Subsequently it was filled with a similar sedimentary succession compared to the older MIS 8 basin. MIS 6 fine-grained and coarse-grained sediments are positioned shallower to their respective MIS 8 counterparts. The age of the overlying younger gravels above the dated MIS 8 glaciofluvial gravel section remains elusive. According to other investigated overdeepened basins, the overlying gravel sediments are most likely significantly younger than the fine-grained basin sediments and associated with the last glaciation (MIS 2–5d). But when taking the older basin generation as a reference, the younger overlying gravels should include a gravel section of MIS 6 age as well. If there is a chronological division in these younger covering gravels, it remains unanswered for now. Potentially clast luminescence dating would shed further light on this question (Jenkins et al., 2018; Serra et al., 2025). But assuming that the same gravel succession is present in the Baierbrunn outcrop, as on top of the Schäftlarn overdeepening (only with varying thicknesses of the sedimentary units), then the sedimentological variation in the Baierbrunn outcrop would suggest chronologically different gravel depositions. Additionally, sedimentary dynamics temporally associated with the LGM most likely influenced the Schäftlarn and Baierbrunn site significantly (van Husen, 2000). Therefore, it seems unlikely that last glaciation deposits are completely absent from Schäftlarn and Baierbrunn. Conversely, the homogenous sedimentology and MSCL logs would not suggest distinctly different sedimentary deposits. However, as previously mentioned, if the source of the gravel deposits remains largely unchanged, it

seems not entirely implausible that significant chronological differences would only be noticeable in slight variations in the content of crystalline and clastic gravel, as well as in the ratio of dolomite and limestone clasts. Besides the weathering features in Baierbrunn between the MIS 8 and most likely MIS 6 glaciofluvial deposits that can be associated with an interglacial period, interglacial sediments are largely missing from the landscape development model. We suggest that they were formed on top of glaciofluvial deposits but eroded by direct glacial or glaciofluvial erosion from the following glacial advance.

6 Conclusions

The sedimentary sequence of the Schäftlarn core deviates from the pattern of other investigated overdeepened structures in the Northern Alpine Foreland. The overdeepened basin of Schäftlarn was filled with glacio-lacustrine sediments during early MIS 8 that were later overlain by glaciofluvial deposits during late MIS 8. This depositional age represents rare evidence of this depositional time frame in the Northern Alpine Foreland. Previously investigated overdeepenings showed a trend towards deposition during MIS 6.

The results of a geophysical reflection seismic survey revealed a younger glacial basin cross-cutting an older glacial basin, from which the drill core was retrieved.

The glaciofluvial outcrop of Baierbrunn – "Münchner Klettergarten" – is younger than previously assumed and can now be attributed to the late MIS 8 at the base. The outcrop can be divided into three sections. This potentially represents a first step in the re-evaluation of the established Quaternary depositional chronology of the Bavarian Alpine Foreland.

The Baierbrunn outcrop and the Schäftlarn core can be parallelised based on luminescence ages and geochemical properties of the deposits.

Data availability. Data will be made available upon reasonable request.

Supplement. The supplement related to this article is available online at https://doi.org/10.5194/egqsj-75-85-2026-supplement.

Author contributions. Luminescence measurements were performed at the VLL by GF, with support and advice from CL. All luminescence age calculations were performed by GF, with support and advice from CL. Text sections, tables, figures and maps were written/compiled by GF with input from all co-authors. Geological and stratigraphical context was provided by EK and MF. Methodological input on the geophysical survey was provided by TB. Interpretation of the geophysical survey was provided by GF, TB and MF. CS provided the clast petrography analysis results. RP conducted the palynological screening. CRN samples were prepared by SN and CS. OM and AW were responsible for the CRN AMS measurements. Subsequent calculation of CRN concentrations and data interpretation was provided by SN. Project set-up and coordination were provided by MF. The paper was reviewed by all co-authors.

Competing interests. At least one of the (co-)authors is a member of the editorial board of *E&G Quaternary Science Journal*. To the best of our knowledge, no conflict of interest, financial or other, exists.

Disclaimer. Publisher's note: Copernicus Publications remains neutral with regard to jurisdictional claims made in the text, published maps, institutional affiliations, or any other geographical representation in this paper. The authors bear the ultimate responsibility for providing appropriate place names. Views expressed in the text are those of the authors and do not necessarily reflect the views of the publisher.

Acknowledgements. This publication is a contribution to ICDP – DOVE and the affiliated project CHATSEIS. Thanks are directed to Flavio Anselmetti, Gerald Gabriel and Frank Preusser for setting up the project. We would like to thank the ICDP Operational Support Group. We are grateful for the gamma spectrometry measurements conducted by Sebastian Schaller and Sönke Szidat. The sedimentology laboratory team at the University of Freiburg is thanked for the grain-size analysis. Julijana Gajic is thanked for her help in obtaining the TIC/TOC results. We are further grateful for the support of the LfU and the operational team at the Hof LfU drill core repository for providing access to the drill core sections. We would like to acknowledge the LIAG (Institute for Applied Geophysics) and the LfU for their contribution to the seismic data acquisition and processing, as well as the municipality of Schäftlarn and the Abbey of Schäftlarn for their support during the field campaign. Jonas Bethke helped with CRN preparation, and Marcel Hirsch is acknowledged for ICP-OES determination. We especially would like to thank the whole DOVE research team for their input and feedback at our regular team meetings and whenever questions needed answering. Additionally, the corresponding author would like to thank the BOKU Doctoral School HADRIAN for supporting his studies and research. Lastly, we would like to thank three reviewers for their constructive comments and Sven Lukas for the editorial handling.

Financial support. This research has been supported by the Eidgenössisches Nuklearsicherheitsinspektorat, the Bayerisches Landesamt für Umwelt, the Deutsche Forschungsgemeinschaft (grant no. 497340281), the Universität für Bodenkultur Wien and Horizon 2020 (grant no. 824096). The travel expenses of the corresponding author and publication costs were provided by the BOKU doctoral school HADRIAN.

Review statement. This paper was edited by Sven Lukas and reviewed by Jürgen Reitner, Tony Reimann and one anonymous referee.

References

Anselmetti, F. S., Bavec, M., Crouzet, C., Fiebig, M., Gabriel, G., Preusser, F., Ravazzi, C., and DOVE scientific team: Drilling Overdeepened Alpine Valleys (ICDP-DOVE): quantifying the age, extent, and environmental impact of Alpine glaciations, Sci. Dril., 31, 51–70, https://doi.org/10.5194/sd-31-51-2022, 2022.

Auclair, M., Lamothe, M., and Huot, S.: Measurement of anomalous fading for feldspar IRSL using SAR, Radiat. Meas., 37, 487–492, https://doi.org/10.1016/S1350-4487(03)00018-0, 2003.

Balco, G. and Rovey, C. W.: An isochron method for cosmogenic-nuclide dating of buried soils and sediments, Am. J. Sci., 308, 1083–1114, https://doi.org/10.2475/10.2008.02, 2008

Bates, M. R., Wenban-Smith, F. F., Bello, S. M., Bridgland, D. R., Buck, L. T., Collins, M. J., Keen, D. H., Leary, J., Parfitt, S. A., Penkman, K., Rhodes, E., Ryssaert, C., and Whittaker, J. E.: Late persistence of the Acheulian in southern Britain in an MIS 8 interstadial: evidence from Harnham, Wiltshire, Quat. Sci. Rev., 101, 159–176, https://doi.org/10.1016/j.quascirev.2014.07.002, 2014.

Batten, D. J.: Reworking of plant microfossils and sedimentary provenance, Geological Society, London, Special Publications, 57, 79–90, https://doi.org/10.1144/GSL.SP.1991.057.01.08, 1991.

Bickel, L., Lüthgens, C., Lomax, J., and Fiebig, M.: Luminescence dating of glaciofluvial deposits linked to the penultimate glaciation in the Eastern Alps, Quat. Int., 357, 110–124, https://doi.org/10.1016/j.quaint.2014.10.013, 2015a.

Bickel, L., Lüthgens, C., Lomax, J., and Fiebig, M.: The timing of the penultimate glaciation in the northern Alpine Foreland: new insights from luminescence dating, Proceedings of the Geologists' Association, 126, 536–550, https://doi.org/10.1016/j.pgeola.2015.08.002, 2015b.

Braucher, R., Del Castillo, P., Siame, L., Hidy, A. J., and Bourles, D. L.: Determination of both exposure time and denudation rate from an in situ-produced 10Be depth profile: A mathematical proof of uniqueness. Model sensitivity and applications to natural cases, Quat. Geochronol., 4, 56–64, https://doi.org/10.1016/j.quageo.2008.06.001, 2009.

Braumann, S. M., Neuhuber, S., Fiebig, M., Schaefer, J. M., Hintersberger, E., and Lüthgens, C.: Challenges in constraining ages of fluvial terraces in the Vienna Basin (Austria) using combined isochron burial and pIRIR225 luminescence dating, Quat. Int., 509, 87–102, https://doi.org/10.1016/j.quaint.2018.01.009, 2019.

Buechi, M. W., Lowick, S. E., and Anselmetti, F. S.: Luminescence dating of glaciolacustrine silt in overdeepened basin fills beyond the last interglacial, Quaternary Geochronology, 37, 55–67, https://doi.org/10.1016/j.quageo.2016.09.009, 2017.

Buechi, M. W., Landgraf, A., Madritsch, H., Mueller, D., Knipping, M., Nyffenegger, F., Preusser, F., Schaller, S., Schnellmann, M., and Deplazes, G.: Terminal glacial overdeepenings: Patterns of erosion, infilling and new constraints on the glaciation history of Northern Switzerland, Quat. Sci. Rev., 344, 108970, https://doi.org/10.1016/j.quascirev.2024.108970, 2024.

Burschil, T.: Seismic measurements, DOVE site 5068_3 (Schäftlarn), Project Chatseis, Survey report, 26 p., Hannover, https://doi.org/10.25928/xpwx-y503, 2024.

Burschil, T., Tanner, D. C., Reitner, J. M., Buness, H., and Gabriel, G.: Unravelling the shape and stratigraphy of a glacially-overdeepened valley with reflection seismic: the Lienz Basin (Austria), Swiss Journal of Geosciences, 112, 341–355, https://doi.org/10.1007/s00015-019-00339-0, 2019.

Buylaert, J. P., Murray, A. S., Thomsen, K. J., and Jain, M.: Testing the potential of an elevated temperature IRSL signal from K-feldspar, Radiation Measurements, 44, 560–565, https://doi.org/10.1016/j.radmeas.2009.02.007, 2009.

Buylaert, J. P., Jain, M., Murray, A. S., Thomsen, K. J., Thiel, C., and Sohbati, R.: A robust feldspar luminescence dating method for Middle and Late Pleistocene sediments, Boreas, 41, 435–451, https://doi.org/10.1111/j.1502-3885.2012.00248.x, 2012.

Chmeleff, J., von Blanckenburg, F., Kossert, K., and Jakob, D.: Determination of the 10Be half-life by multicollector ICP-MS and liquid scintillation counting, Nuclear Instruments and Methods in Physics Research, Section B, Beam Interactions with Materials and Atoms, 268, 192–199, https://doi.org/10.1016/j.nimb.2009.09.012, 2010.

Cunningham, A. C. and Wallinga, J.: Realizing the potential of fluvial archives using robust OSL chronologies, Quaternary Geochronology, 12, 98–106, https://doi.org/10.1016/j.quageo.2012.05.007, 2012.

Davies, B. J., Roberts, D. H., Bridgland, D. R., Cofaigh, C.Ó, Riding, J. B., Demarchi, B., Penkman, K. E. H., and Pawley, S. M.: Timing and depositional environments of a Middle Pleistocene glaciation of northeast England: New evidence from Warren House Gill, County Durham, Quat. Sci. Rev., 44, 180–212, https://doi.org/10.1016/j.quascirev.2010.02.003, 2012.

Dehnert, A., Lowick, S. E., Preusser, F., Anselmetti, F. S., Drescher-Schneider, R., Graf, H. R., Heller, F., Horstmeyer, H., Kemna, H. A., Nowaczyk, N. R., Züger, A., and Furrer, H.: Evolution of an overdeepened trough in the northern Alpine Foreland at Niederweningen, Switzerland, Quat. Sci. Rev., 34, 127–145, https://doi.org/10.1016/j.quascirev.2011.12.015, 2012.

Doben, K., Doppler, G., Freudenberger, W., Jerz, H., Meyer, R. K. F., Mielke, H., Ott, W.-D., Rohrmüller, J., Schmidt-Kaler, H., Schwerd, K., and Unger, H. J.: Geologische Karte von Bayern 1 : 500 000, 4. Auflage, München, 1996.

Doppler, G., Kroemer, E., Rögner, K., Wallner, J., Jerz, H., and Grottenthaler, W.: Quaternary Stratigraphy of Southern Bavaria, E&G Quaternary Sci. J., 60, 23, https://doi.org/10.3285/eg.60.2-3.08, 2011.

Dreesbach, R.: Sedimentpetrographische Untersuchungen zur Stratigraphie des Würmglazials im Bereich des Isar-Loisachgletschers, Dissertation Ludwig-Maximilians-Universität München, 1985.

Dreesbach, R.: Zur Lithostratigraphie des Würmglazials im Gebiet des Isar-Loisach-Gletschers / Oberbayern, Z. dt. geol. Ges., 137, 553–572, 1986.

Duller, G. A. T.: Single-grain optical dating of Quaternary sediments: why aliquot size matters in luminescence dating, Boreas, 37, 589–612, https://doi.org/10.1111/j.1502-3885.2008.00051.x, 2008.

Ellwanger, D., Wielandt-Schuster, U., Franz, M., and Simon, T.: The Quaternary of the southwest German Alpine Foreland (Bodensee-Oberschwaben, Baden-Württemberg, Southwest Germany), E&G Quaternary Sci. J., 60, 22, https://doi.org/10.3285/eg.60.2-3.07, 2011.

Erlanger, E. D., Granger, D. E., and Gibbon, R. J.: Rock uplift rates in South Africa from isochron burial dating of fluvial and marine terraces, Geology, 40, 1019–1022, https://doi.org/10.1130/G33172.1, 2012.

Fenton, C. R., Binnie, S. A., Dunai, T., and Niedermann, S.: The SPICE project: Calibrated cosmogenic ^{26}Al production rates and cross-calibrated ^{26}Al/^{10}Be, ^{26}Al/^{14}C, and ^{26}Al/^{21}Ne ratios in quartz from the SP basalt flow, AZ, USA, Quat. Geochron., 67, 101218, https://doi.org/10.1016/j.quageo.2021.101218, 2022.

Fernández Mosquera, D., Marti, K., Vidal Romaní, J. R., and Weigel, D.: Late Pleistocene deglaciation chronology in the NW of the Iberian Peninsula using cosmic-ray produced ^{21}Ne in quartz, Nuclear Instruments and Methods in Physical Research B: Beam Interactions with Materials and Atoms, 172, 832–837, https://doi.org/10.1016/S0168-583X(00)00339-6, 2000.

Firla, G., Lüthgens, C., Neuhuber, S., Schmalfuss, C., Kroemer, E., Preusser, F., and Fiebig, M.: Analyzing complex single grain feldspar equivalent dose distributions for luminescence dating of glacially derived sediments, Quaternary Geochronology, 85, 101627, https://doi.org/10.1016/j.quageo.2024.101627, 2024a.

Firla, G., Lüthgens, C., Preusser, F., and Fiebig, M.: Unravelling the chronology of the infill of glacially overdeepened structures in the northern foreland of the European Alps [Poster], 37th International Geological Congress, Busan, Republic of Korea (South Korea), 25–31 August 2024, T2 Quaternary Geology – S3 Current and future directions in Quaternary chronostratigraphy, 2024b.

Galbraith, R., Roberts, R., Laslett, G., Yoshida, H., and Olley, J.: Optical dating of single and multiple grains of quartz from Jinmium Rock Shelter, Northern Australia: part I, experimental design and statistical models, Archaeometry, 41, 339–364, https://doi.org/10.1111/j.1475-4754.1999.tb00987.x, 1999.

Gegg, L. and Preusser, F.: Comparison of overdeepened structures in formerly glaciated areas of the northern Alpine foreland and northern central Europe, E&G Quaternary Sci. J., 72, 23–36, https://doi.org/10.5194/egqsj-72-23-2023, 2023.

Gegg, L., Salcher, B. C., Pollhammer, T., Cohen, D., Fischer, U. H., and Landgraf, A.: An inventory of subglacial overdeepenings in southern Germany and Austria, Boreas, https://doi.org/10.1111/bor.12693, 2025.

Giraudi, C. and Giaccio, B.: Middle Pleistocene glaciations in the Apennines, Italy: new chronological data and preservation of the glacial record, Geological Society, London, Special Publications, 433, 161–178, https://doi.org/10.1144/SP433.1, 2017.

Granger, D. E.: A review of burial dating methods using 26Al and 10Be, Geological Society of America Special Papers, 415, 1–16, https://doi.org/10.1130/2006.2415(01), 2006.

Granger, D. E.: Cosmogenic nuclide burial dating in archaeology and paleoanthropology, in: Treatise on Geochemistry (2nd edn.), edited by: Holland H. D. and Turekian K. K., Oxford: Elsevier, 14, 81–97, https://doi.org/10.1016/B978-0-08-095975-7.01208-0, 2014.

Heisinger, B., Lal, D., Jull, A. J. T., Kubik, P., Ivy-Ochs, S., Neumaier, S., Knie, K., Lazarev, V., and Nolte, E.: Production of selected cosmogenic radionuclides by muons: 1. Fast muons, Earth and Planetary Science Letters, 200, 345–355, https://doi.org/10.1016/S0012-821X(02)00640-4, 2002a.

Heisinger, B., Lal, D., Jull, A. J. T., Kubik, P., Ivy-Ochs, S., Knie, K., and Nolte, E.: Production of selected cosmogenic radionuclides by muons: 2. Capture of negative muons, Earth and Planetary Sci. Lett. , 200, 357–369, https://doi.org/10.1016/S0012-821X(02)00641-6, 2002b.

Hughes, P. D., Woodward, J. C., van Calsteren, P. C., and Thomas, L. E.: The glacial history of the Dinaric Alps, Montenegro, Quat. Sci. Rev., 30, 3393–3412, https://doi.org/10.1016/j.quascirev.2011.08.016, 2011.

Hughes, P. D., Gibbard, P. L., and Ehlers, J.: The "missing glaciations" of the Middle Pleistocene, Quaternary Res., 96, 161–183, https://doi.org/10.1017/qua.2019.76, 2020.

Huntley, D. and Baril, M.: The K content of the K-feldspars being measured in optical dating or in thermoluminescence dating, Ancient TL, 15, 11–13, 1997.

Jenkins, G. T. H., Duller, G. A. T., Roberts, H. M., Chiverrell, R. C., and Glasser, N. F.: A new approach for luminescence dating glaciofluvial deposits – High precision optical dating of cobbles, Quat. Sci. Rev., 192, 263–273, https://doi.org/10.1016/j.quascirev.2018.05.036, 2018.

Jerz, H.: Das Wolfratshausener Becken: seine glaziale Anlage und Übertiefung, E&G Quaternary Sci. J., 29, 63–70, https://doi.org/10.3285/eg.29.1.06, 1979.

Jerz, H.: Das Eiszeitalter in Bayern – Erdgeschichte, Gesteine, Wasser, Boden. – Geologie von Bayern, 2, Stuttgart, 1993.

Jerz, H., Bader, K., Baumann, H. J., Kovanda, J., Müller, J., Kleinmann, A., Schauer, T., Schmeidl, H., and Wrobel, J.-P.: Geologische Karte von Bayern 1 : 25 000 – Erläuterungen zum Blatt Nr. 8034 Starnberg Süd, München, 1987.

Kars, R. H., Busschers, F. S., and Wallinga, J.: Validating post IR-IRSL dating on K-feldspars through comparison with quartz OSL ages, Quat. Geochron., 12, 74–86, https://doi.org/10.1016/j.quageo.2012.05.001, 2012.

Klasen, N.: Lumineszenzdatierung glazifluvialer Sedimente im nördlichen Alpenvorland (Luminescence Dating of Glaciofluvial Sediments in the Northern Alpine Foreland), Dissertation Universität zu Köln, 2008.

Korschinek, G., Bergmaier, A., Faestermann, T., Gerstmann, U. C., Knie, K., Rugel, G., Wallner, A., Dillmann, I., Dollinger, G., Lierse von Gostomski, Ch., Kossert, K., Maiti, M., Poutivtsev, M., and Remmert, A.: A new value for the half-life of 10Be by heavy-ion elastic recoil detection and liquid scintillation counting, Nuclear Instruments and Methods in Physics Research, Section B, Beam Interactions with Materials and Atoms, 268, 187–191, https://doi.org/10.1016/j.nimb.2009.09.020, 2010.

Kreutzer, S., Schmidt, C., Fuchs, M. C., Dietze, M., and Fuchs, M.: Introducing an R package for luminescence dating analysis, Ancient TL, 30, 1–8, 2012.

Kulig, G.: Erstellung einer Auswertesoftware zur Altersbestimmung mittels Lumineszenzverfahren unter spezieller Berücksichtigung des Einflusses radioaktiver Ungleichgewichte in der 238-U-Zerfallsreihe, in: Bakkalaureusarbeit Network Computing, TU Freiberg, 2005.

Lachner, J., Martschini, M., Kalb, A., Kern, M., Marchhart, O., Plasser, F., Priller, A., Steier, P., Wieser, A., and Golser, R.: Highly sensitive 26Al measurements by Ion-Laser-InterAction Mass Spectrometry, International Journal of Mass Spectrometry, 465, 116576, https://doi.org/10.1016/j.ijms.2021.116576, 2021.

Lauer, T. and Weiss, M.: Timing of the Saalian- and Elsterian glacial cycles and the implications for Middle – Pleis-

tocene hominin presence in central Europe, Sci. Rep., 8, 5111, https://doi.org/10.1038/s41598-018-23541-w, 2018.

Lisiecki, L. E. and Raymo, M. E.: A Pliocene-Pleistocene stack of 57 globally distributed benthic $\delta^{18}O$ records, Paleoceanography, 20, PA1003, https://doi.org/10.1029/2004PA001071, 2005.

Lomax, J., Wolf, D., Meliksetian, K., Wolpert, T., Sahakyan, L., Hovakimyan, H., Faust, D., and Fuchs, M.: Testing post-IR-IRSL dating on Armenian loess-palaeosol sections against independent age control, Quat. Geochron., 69, 101265, https://doi.org/10.1016/j.quageo.2022.101265, 2022.

Lowick, S. E., Buechi, M. W., Gaar, D., Graf, H. R., and Preusser, F.: Luminescence dating of middle pleistocene proglacial deposits from northern Switzerland: methodological aspects and stratigraphical conclusions, Boreas, 44, 459–482, https://doi.org/10.1111/bor.12114, 2015.

Marks, L., Woronko, B., Majecka, A., Rylova, T., Orłowska, A., Hrachanik, M., Rychel, J., Zbucki, L., Bahdasarau, M., Hradunova, A., Nitychoruk, J., Nowacki, L., and Pochocka-Szwarc, K.: Middle Pleistocene deposits at Rechitsa, western Belarus, and their input to MIS 12-6 stratigraphy in central Europe, Quat. Int., 553, 34–52, https://doi.org/10.1016/j.quaint.2020.07.022, 2020.

Mueller, D., Gegg, L., Fülling, A., Buechi, M. W., Deplazes, G., and Preusser, F.: Luminescence dating of glacially sourced deposits from northern Switzerland: Comparing multigrain aliquots and single grains of quartz and feldspar, Quaternary Geochronology, 82, 101551, https://doi.org/10.1016/j.quageo.2024.101551, 2024.

Nishiizumi, K.: Preparation of 26Al AMS standards, Nuclear Instruments and Methods in Physics Research, Section B, Beam Interactions with Materials and Atoms, 223–224, 388–392, https://doi.org/10.1016/s0168-583x(04)00600-7, 2004.

Penck, A. and Brückner, E.: Die Alpen im Eiszeitalter. Tauchnitz, Leipzig, 1909.

Pini, R. and Bertuletti, P.: Palaeoecological analysis of terrestrial biological proxies on sediment samples from the Schäftlarn core (ICDP core 5068_3_A), Scientific report IGAG Milano, 2023.

Prescott, J. and Stephan, L.: The contribution of cosmic radiation to the environmental dose for thermoluminescence dating - Latitude, altitude and depth dependencies, PACT, 6, 17–25, 1982.

Prescott, J. R. and Hutton, J. T.: Cosmic ray contributions to dose rates for luminescence and ESR dating: Large depths and long-term time variations, Radiat. Meas., 23, 497–500, https://doi.org/10.1016/1350-4487(94)90086-8, 1994.

Preusser, F. and Kasper, H. U.: Comparison of dose rate determination using high-resolution gamma spectrometry and inductively coupled plasma-mass spectrometry, Ancient TL, 19, 19–23, https://doi.org/10.26034/la.atl.2001.329, 2001.

Preusser, F., Drescher-Schneider, R., Fiebig, M., and Schlüchter, C.: Re-interpretation of the Meikirch pollen record, Swiss Alpine Foreland, and implications for Middle Pleistocene chronostratigraphy, J. Quaternary Sci., 20, 607–620, https://doi.org/10.1002/jqs.930, 2005.

Preusser, F., Reitner, J. M., and Schlüchter, C.: Distribution, geometry, age and origin of overdeepened valleys and basins in the Alps and their foreland, Swiss J. Geosci., 103, 407–426, https://doi.org/10.1007/s00015-010-0044-y, 2010.

Preusser, F., Graf, H. R., Keller, O., Krayss, E., and Schlüchter, C.: Quaternary glaciation history of northern Switzerland, E&G Quaternary Sci. J., 60, 21, https://doi.org/10.3285/eg.60.2-3.06, 2011.

Rades, E. F., Fiebig, M., and Lüthgens, C.: Luminescence dating of the Rissian type section in southern Germany as a base for correlation, Quat. Int., 478, 38–50, https://doi.org/10.1016/J.QUAINT.2016.07.055, 2018.

Reimann, T., Thomsen, K. J., Jain, M., Murray, A. S., and Frechen, M.: Single-grain dating of young sediments using the pIRIR signal from feldspar, Quaternary Geochronology, 11, 28–41, https://doi.org/10.1016/j.quageo.2012.04.016, 2012.

Reitner, J. M.: The Imprint of Quaternary Processes on the Austrian Landscape, in: Landscapes and Landforms of Austria, edited by: Embleton-Hamann, C., World Geomorphological Landscapes, Springer, Cham, https://doi.org/10.1007/978-3-030-92815-5_3, 2022.

Reuther, A. U., Fiebig, M., Ivy-Ochs, S., Kubik, P. W., Reitner, J. M., Jerz, H., and Heine, K.: Deglaciation of a large piedmont lobe glacier in comparison with a small mountain glacier – new insight from surface exposure dating. Two studies from SE Germany, E&G Quaternary Sci. J., 60, 18, https://doi.org/10.3285/eg.60.2-3.03, 2011.

Roskosch, J., Winsemann, J., Polom, U., Brandes, C., Tsukamoto, S., Weitkamp, A., Bartholomäus, W. A., Henningsen, D., and Frechen, M.: Luminescence dating of ice-marginal deposits in northern Germany: evidence for repeated glaciations during the Middle Pleistocene (MIS 12 to MIS 6), Boreas, 44, 103–126, https://doi.org/10.1111/bor.12083, 2014.

Rugel, G., Pavetich, S., Akhmadaliev, S., Enamorado-Baez, S. M., Scharf, A., Ziegenrücker, R., and Merchel, S.: The first four years of the AMS-facility DREAMS: Status and developments for more accurate radionuclide data, Nuclear Instruments and Methods in Physics Research Section B: Beam Interactions with Materials and Atoms, 370, 94–100, https://doi.org/10.1016/j.nimb.2016.01.012, 2016.

Ruszkiczay-Rüdiger, Z., Neuhuber, S., Hintersberger, E., and Nørgaard, J.: Iterative outlier identification for robust cosmogenic burial dating of fluvial terraces: a case study from the Danube River (Vienna Basin, Austria), E&G Quaternary Sci. J., 74, 59–78, https://doi.org/10.5194/egqsj-74-59-2025, 2025.

Ruszkiczay-Rüdiger, Zs., Neuhuber, S., Braucher, R., Lachner, J., Steier, P., Wieser, A., Braun, M., and ASTER Team.: Comparison and performance of two cosmogenic nuclide sample preparation procedures of in situ produced 10Be and 26Al, Journal of Radioanalytical and Nuclear Chemistry, 329, 1523–1536, https://doi.org/10.1007/s10967-021-07916-4, 2021.

Salcher, B. C., Starnberger, R., and Götz, J.: The last and penultimate glaciation in the North Alpine Foreland: New stratigraphical and chronological data from the Salzach Glacier, Quat. Int., 388, 218–231, https://doi.org/10.1016/j.quaint.2015.09.076, 2015.

Schaller, S., Buechi, M. W., Schuster, B., and Anselmetti, F. S.: Drilling into a deep buried valley (ICDP DOVE): a 252 m long sediment succession from a glacial overdeepening in northwestern Switzerland, Sci. Dril., 32, 27–42, https://doi.org/10.5194/sd-32-27-2023, 2023.

Schuster, B., Gegg, L., Schaller, S., Buechi, M. W., Tanner, D. C., Wielandt-Schuster, U., Anselmetti, F. S., and Preusser, F.: Shaped and filled by the Rhine Glacier: the overdeepened Tan-

nwald Basin in southwestern Germany, Sci. Dril., 33, 191–206, https://doi.org/10.5194/sd-33-191-2024, 2024.

Schuster, R., Egger, H., Krenmayr, H. G., Linner, M., Mandl, G. W., Matura, A., Nowotny, A., Pascher, G., Pestal, G., Pistotnik, J., Rockenschaub, M., and Schnabel, W.: Geologische Übersichtskarte der Republik Österreich 1 : 1 500 000, Geologische Bundesanstalt, Wien, 2015.

Serra, E., Mueller, D., Gegg, L., Firla, G., Piccoli, F., Hergarten, S., Margirier, A., and Preusser, F.: Combined single grain and cobble luminescence dating of poorly bleached glaciofluvial deposits from the Swiss Alpine foreland, Quaternary Geochronology, 87, 101650, https://doi.org/10.1016/j.quageo.2025.101650, 2025.

Steier, P., Martschini, M., Buchriegler, J., Feige, J., Lachner, J., Merchel, S., Michlmayr, L., Priller, A., Rugel, G., Schmidt, E., Wallner, A., Wild, E. M., and Golser, R.: Comparison of methods for the detection of 10Be with AMS and a new approach based on a silicon nitride foil stack, International Journal of Mass Spectrometry, 444, 116175, https://doi.org/10.1016/j.ijms.2019.116175, 2019.

Stockmarr, J.: Tablets with spores used for absolute pollen analysis, Pollen et Spores, 13, 615–620, 1971.

Streel, M. and Bless, M. J. M.: Occurrence and significance of reworked palynomorphs, Med. Rijks. Geol. Dienst., 32–10, 69–80, 1980.

Thiel, C., Buylaert, J.-P., Murray, A., Terhorst, B., Hofer, I., Tsukamoto, S., and Frechen, M.: Luminescence dating of the Stratzing loess profile (Austria) – Testing the potential of an elevated temperature post-IR IRSL protocol, Quat. Int., 234, 23–31, https://doi.org/10.1016/j.quaint.2010.05.018, 2011.

van Husen, D.: Geological Processes during the Quaternary, Mittl. Österreichischen Geol. Ges., 92, 135–156, 2000.

Vidal, R., Fernández Mosquera, D., and Marti, K.: The glaciation of Serra de Queixa-Invernadoiro and Serra do Gerês-Xurés, NW Iberia. A critical review and a cosmogenic nuclide (^{10}Be and ^{21}Ne) chronology, Cadernos Laboratorio Xeolóxico de Laxe, 38, 27–45, https://doi.org/10.17979/cadlaxe.2015.38.0.3681, 2015.

White, T. S., Bridgland, D. R., Westaway, R., and Straw, A.: Evidence for late Middle Pleistocene glaciation of the British margin of the southern North Sea, J. Quat. Sci., 32, 261–275, https://doi.org/10.1002/jqs.2826, 2017.

Wintle, A. G. and Murray, A. S.: A review of quartz optically stimulated luminescence characteristics and their relevance in single-aliquot regeneration dating protocols, Radiation Measurements, 41, 369–391, https://doi.org/10.1016/j.radmeas.2005.11.001, 2006.